Shear Wave Propagation and Band Gaps in Finitely Deformed Dielectric Elastomer Laminates: Long Wave Estimates and Exact Solution

Pavel I. Galich
Department of Aerospace Engineering,
Technion—Israel Institute of Technology,
Haifa 32000, Israel

Stephan Rudykh
Department of Aerospace Engineering,
Technion—Israel Institute of Technology,
Haifa 32000, Israel
e-mail: rudykh@technion.ac.il

We analyze small amplitude shear waves (SWs) propagating in dielectric elastomer (DE) laminates subjected to finite deformations and electrostatic excitations. First, we derive long wave estimates for phase and group velocities of the shear waves propagating in any direction in DE laminates subjected to any homogenous deformation in the presence of an electric filed. To this end, we utilize a micromechanics-based energy potential for layered media with incompressible phases described by neo-Hookean ideal DE model. The long wave estimates reveal the significant influence of electric field on the shear wave propagation. However, there exists a configuration, for which electric field does not influence shear waves directly, and can only alter the shear waves through deformation. We study this specific configuration in detail, and derive an exact solution for the steady-state small amplitude waves propagating in the direction perpendicular to the finitely deformed DE layers subjected to electrostatic excitation. In agreement with the long wave estimate, the exact dispersion relation and the corresponding shear wave band gaps (SBGs)—forbidden frequency regions—are not influenced by electric field. However, SBGs in DE laminates with highly nonlinear electroelastic phases still can be manipulated by electric field through electrostatically induced deformation. In particular, SBGs in DE laminates with electroelastic Gent phases widen and shift toward higher frequencies under application of an electric field perpendicular to the layers. However, in laminates with neo-Hookean ideal DE phases, SBGs are not influenced either by electric field or by deformation. This is due to the competing mechanisms of two governing factors: changes in geometry and material properties induced by deformation. In this particular case, these two competing factors entirely cancel each other.
[DOI: 10.1115/1.4037159]

Keywords: dielectric elastomers, layered materials, wave propagation, finite deformations, band gaps

1 Introduction

Dielectric elastomers (DEs) can develop large deformations when excited by an external electric field [1]. Therefore, these artificial muscles are of great interest for various applications, such as soft robotics [2], various actuators [3,4], energy generators [5,6], to name a few. It has been recently shown that large deformations can significantly influence wave propagation even in relatively simple deformable materials without electromechanical coupling [7–10]. In turn, DEs offer a way to manipulate elastic waves via application of an external electric field. Thus, for example, the effect has been used to control wave propagation in homogenous DEs [11–13]. Moreover, microstructured DEs hold even greater potential for active control of elastic waves by an electric field [14,15]. Hence, investigation of wave propagation in composite DEs opens new possibilities in improving of small length-scale devices, for example, micro-electromechanical systems, where an electric field is the preferred operated variable.

Following the work of Toupin [16], the theory of nonlinear electroelasticity for homogeneous isotropic hyperelastic media has been revised recently by Dorfmann and Ogden [17], McMeeking and Landis [18], and Suo et al. [19]. More recently, Cohen et al. [20] proposed a model based on considerations of polymer networks under electromechanical loadings. Motivated by potential enhancement of electromechanical coupling, which is typically rather weak in DEs, microstructured DEs have been explored [21–23] showing significant potential of this approach. We note that microstructured DEs may develop instabilities at different length scales [24–28].

The analysis of small amplitude wave propagation in finitely deformed nonlinear electroelastic materials in the presence of an electric field in the frame of the quasi-electrostatic approximation was presented by Dorfmann and Ogden [29]. This paper has been followed by a number of works on elastic wave propagation in finitely deformed homogenous and composite DEs [11–13,30]. Note that layered DEs are of specific importance since they may be realized through various layer-by-layer material fabrication techniques, which already allow manufacturing of deformable layered materials across length scales [31–33]. However, the existing literature on elastic wave propagation in finitely deformed DE laminates in the presence of an electric field reports some contradictory results. In particular, Shmuel and deBotton [30] considered shear wave band gap (SBGs) structures in DE laminates with ideal dielectric neo-Hookean incompressible phases, and they

Contributed by the Applied Mechanics Division of ASME for publication in the Journal of Applied Mechanics. Manuscript received April 11, 2017; final manuscript received June 17, 2017; published online July 7, 2017. Assoc. Editor: Daining Fang.

reported that these SBGs alter under application of an external electric field. However, our results clearly show that the SBGs in the neo-Hookean DE laminates are not influenced either by electric field or by induced deformation. We note that our results agree with the exact solution for the long waves in DE laminates. Moreover, the derived dispersion relation reduces to the classical result for linear elastic layered media [34] in the absence of an electric field and deformation. We should note that Shmuel and deBotton [35] have just published the corrigendum reporting that the SBGs in the neo-Hookean DEs are shifted by electric field toward higher frequencies. However, these new results by Shmuel and deBotton [35] do not agree with the exact solution for long waves and with the exact solution for any wavelengths as detailed in the Appendix.

To shed light on the influence of electric field on shear waves in DE laminates, we analyze small amplitude shear wave propagating in DE layered media comprised of two alternating isotropic incompressible electroelastic phases. First, we derive the long wave estimates for phase and group velocities of shear waves propagating in any direction in DE laminates undergoing any homogenous deformation in the presence of an electric field. To this end, we make use of an exact solution for finitely deformed DE laminates allowing us to express an effective energy potential in terms of microstructure parameters and physical properties of the constituents. These estimates reveal the significant dependence of the shear wave characteristics on electric field and deformation. However, we found that there is a unique configuration—when elastic waves propagate perpendicular to the layers—for which phase and group velocities are independent of electric field, and these acoustic characteristics can be influenced only through electrostatically induced deformations. This holds true for any direction of an applied electric field. Again, for any other direction of propagation, the phase and group velocities explicitly depend on electric field. We further analyze this specific configuration and derive the dispersion relation for the small amplitude shear waves propagating perpendicular to finitely deformed layers with electric field applied perpendicular to the layers. The derived dispersion relation is shown to be of the same form as the relation for hyperelastic laminates [36] undergoing finite deformations in the absence of an electric field. Thus, shear waves propagating perpendicular to the layers in DE laminates are not affected by electric field directly, and they can be influenced by electric field only through induced deformations. Note that this result is in full agreement with the exact solution for long waves. Finally, we analyze SBGs in DE laminates by making use of the derived dispersion relation. In particular, we show that SBGs widen and shift up toward higher frequencies in DE laminates with ideal dielectric Gent phases subjected to an electric field through the thickness of the layers. Once again, SBGs in the DE laminates with neo-Hookean ideal dielectric phases do not depend on electric field.

2 Theoretical Background

To describe finite deformations of a continuous electroelastic body occupying Ω_0 and Ω_t domains in the reference and current configurations, respectively, we introduce the deformation gradient $\mathbf{F}(\mathbf{X},t)=\partial\mathbf{x}(\mathbf{X},t)/\partial\mathbf{X}$, where $\mathbf{X}$ and $\mathbf{x}$ are position vectors in the reference and current configurations, respectively. Then, the Jacobian $J\equiv \det\mathbf{F}>0$ defines the volume change of the body with respect to the reference state.

2.1 Electrostatics. In this work, we adopt the so-called quasi-electrostatic approximation assuming the absence of magnetic fields and neglecting electromagnetic interactions. Thus, in the absence of free body charges and currents, the equations of electrostatics in the current configuration read as

$$\mathrm{div}\mathbf{D}=0 \ \text{ and } \ \mathrm{curl}\mathbf{E}=\mathbf{0} \tag{1}$$

where $\mathbf{D}$ and $\mathbf{E}$ denote electric displacement and electric field applied in the current configuration, respectively. Here and thereafter, the differential operators with the first low-case letter refer to the current configuration, while the differential operators with the first upper-case letter refer to the reference configuration.

In the reference configuration, the equations of electrostatics read as

$$\mathrm{Div}\mathbf{D}_L=0 \ \text{ and } \ \mathrm{Curl}\mathbf{E}_L=\mathbf{0} \tag{2}$$

where

$$\mathbf{D}_L=J\mathbf{F}^{-1}\cdot\mathbf{D} \ \text{ and } \ \mathbf{E}_L=\mathbf{F}^T\cdot\mathbf{E} \tag{3}$$

are the Lagrangian counterparts of $\mathbf{D}$ and $\mathbf{E}$, respectively.

2.2 Mechanical Balance Laws. In the absence of body forces, the linear and angular momentum balance for an electroelastic material are

$$\mathrm{div}\boldsymbol{\tau}=\rho\mathbf{x}_{,tt} \ \text{ and } \ \boldsymbol{\tau}=\boldsymbol{\tau}^T \tag{4}$$

where $\boldsymbol{\tau}$ represents the *total* Cauchy stress tensor and ρ is the mass density of the material in the current configuration.

In Lagrangian description, the balance equations (4) read as

$$\mathrm{Div}\mathbf{P}=\rho_0\mathbf{x}_{,tt} \ \text{ and } \ \mathbf{P}\cdot\mathbf{F}^T=\mathbf{F}\cdot\mathbf{P}^T \tag{5}$$

where

$$\mathbf{P}=J\boldsymbol{\tau}\cdot\mathbf{F}^{-T} \ \text{ and } \ \rho_0=J\rho \tag{6}$$

are the first Piola–Kirchhoff *total* stress tensor and the mass density of the material in the reference configuration, respectively.

2.3 Constitutive Equations. To model nonlinear behavior of DEs, we consider an energy potential $\psi(\mathbf{F},\mathbf{D}_L)$, as introduced in Dorfmann and Ogden [17]. The strain energy-density potential is a function of deformation gradient $\mathbf{F}$ and Lagrangian counterpart of electric displacement $\mathbf{D}_L$. Then, for an electroelastic material, the first Piola–Kirchhoff total stress tensor and Lagrangian counterpart of electric field are given by

$$\mathbf{P}=\frac{\partial\psi}{\partial\mathbf{F}} \quad \text{and} \quad \mathbf{E}_L=\frac{\partial\psi}{\partial\mathbf{D}_L} \tag{7}$$

For an incompressible material, $J=1$, and the constitutive equations (7) modify as

$$\mathbf{P}=\frac{\partial\psi}{\partial\mathbf{F}}-p\mathbf{F}^{-T} \quad \text{and} \quad \mathbf{E}_L=\frac{\partial\psi}{\partial\mathbf{D}_L} \tag{8}$$

where p denotes an unknown Lagrange multiplier.

2.4 Incremental Equations. For an electroelastic material, the incremental constitutive equations for the first Piola–Kirchhoff stress and Lagrangian electric field read as

$$\dot{\mathbf{P}}=\mathbb{C}_0:\dot{\mathbf{F}}+\boldsymbol{\mathcal{M}}_0\cdot\dot{\mathbf{D}}_L \quad \text{and} \quad \dot{\mathbf{E}}_L=\dot{\mathbf{F}}:\boldsymbol{\mathcal{M}}_0+\mathbf{K}_0\cdot\dot{\mathbf{D}}_L \tag{9}$$

respectively. Here, the superposed dot represent incremental changes in the corresponding variables; $\mathbb{C}_0$, $\boldsymbol{\mathcal{M}}_0$, and $\mathbf{K}_0$ are the tensors of electroelastic moduli defined as

$$\mathbb{C}_0=\frac{\partial^2\psi}{\partial\mathbf{F}\partial\mathbf{F}}, \quad \boldsymbol{\mathcal{M}}_0=\frac{\partial^2\psi}{\partial\mathbf{F}\partial\mathbf{D}_L} \quad \text{and} \quad \mathbf{K}_0=\frac{\partial^2\psi}{\partial\mathbf{D}_L\partial\mathbf{D}_L} \tag{10}$$

For an incompressible material, the incremental equations (9) read as

$$\dot{\mathbf{P}} = \mathbb{C}_0 : \dot{\mathbf{F}} + p\mathbf{F}^{-T}\cdot\dot{\mathbf{F}}^{T}\cdot\mathbf{F}^{-T} - \dot{p}\mathbf{F}^{-T} + \boldsymbol{\mathcal{M}}_0\cdot\dot{\mathbf{D}}_L \quad \text{and} \quad \dot{\mathbf{E}}_L = \dot{\mathbf{F}} : \boldsymbol{\mathcal{M}}_0 + \mathbf{K}_0\cdot\dot{\mathbf{D}}_L \tag{11}$$

2.5 Incremental Motions Superimposed on Finite Deformation in the Presence of an Electric Field. In the frame of the updated Lagrangian formulation, the incremental forms of the governing Eqs. (2) and $(5)_1$, describing small motions superimposed on finite deformation, transform to

$$\mathrm{div}\dot{\mathbf{D}}_{L\star} = 0, \quad \mathrm{curl}\dot{\mathbf{E}}_{L\star} = \mathbf{0}, \text{ and } \mathrm{div}\dot{\mathbf{P}}_{\star} = \rho\ddot{\mathbf{x}}_{,tt} \tag{12}$$

where

$$\dot{\mathbf{D}}_{L\star} = J^{-1}\mathbf{F}\cdot\dot{\mathbf{D}}_L, \quad \dot{\mathbf{E}}_{L\star} = \mathbf{F}^{-T}\cdot\dot{\mathbf{E}}_L, \text{ and } \dot{\mathbf{P}}_{\star} = J^{-1}\dot{\mathbf{P}}\cdot\mathbf{F}^{T} \tag{13}$$

are the so-called push-forward versions of $\dot{\mathbf{D}}_L$, $\dot{\mathbf{E}}_L$, and $\dot{\mathbf{P}}$, respectively. Identifying the field of incremental displacements as $\mathbf{u} = \dot{\mathbf{x}}$ and then displacement gradient as $\mathbf{H} = \mathrm{grad}\mathbf{u} = \dot{\mathbf{F}}\cdot\mathbf{F}^{-1}$, we obtain the following updated incremental relations (9):

$$\dot{\mathbf{P}}_{\star} = \mathbb{C} : \mathbf{H} + \boldsymbol{\mathcal{M}}\cdot\dot{\mathbf{D}}_{L\star} \quad \text{and} \quad \dot{\mathbf{E}}_{L\star} = \mathbf{H} : \boldsymbol{\mathcal{M}} + \mathbf{K}\cdot\dot{\mathbf{D}}_{L\star} \tag{14}$$

where

$$\mathbb{C}_{irks} = J^{-1}\mathbb{C}_{0ijkl}F_{rj}F_{sl}, \quad \mathcal{M}_{irk} = \mathcal{M}_{0ijm}F_{rj}F^{-1}_{mk} \quad \text{and} \quad \mathbf{K} = J\mathbf{F}^{-T}\cdot\mathbf{K}_0\cdot\mathbf{F}^{-1} \tag{15}$$

are the updated tensors of electroelastic moduli, possessing the following symmetries:

$$\mathbb{C}_{irks} = \mathbb{C}_{ksir}, \quad \mathcal{M}_{irk} = \mathcal{M}_{rik}, \quad \text{and} \quad \mathbf{K} = \mathbf{K}^{T} \tag{16}$$

For an incompressible material, the incremental equations (14) read as

$$\dot{\mathbf{P}}_{\star} = \mathbb{C} : \mathbf{H} + p\mathbf{H}^{T} - \dot{p}\mathbf{I} + \boldsymbol{\mathcal{M}}\cdot\dot{\mathbf{D}}_{L\star} \quad \text{and} \quad \dot{\mathbf{E}}_{L\star} = \mathbf{H} : \boldsymbol{\mathcal{M}} + \mathbf{K}\cdot\dot{\mathbf{D}}_{L\star} \tag{17}$$

moreover, the incompressibility assumption implies

$$\mathrm{tr}\mathbf{H} \equiv \mathrm{div}\,\mathbf{u} = 0 \tag{18}$$

2.6 Plane Waves in Incompressible DEs Subjected to Electromechanical Loading. We seek for solution of Eq. (12) in the form of plane waves with constant polarizations [29]

$$\mathbf{u} = \mathbf{g}f(\mathbf{n}\cdot\mathbf{x} - ct), \quad \dot{\mathbf{D}}_{L\star} = \mathbf{d}g(\mathbf{n}\cdot\mathbf{x} - ct), \quad \text{and} \quad \dot{p} = \Pi(\mathbf{n}\cdot\mathbf{x} - ct) \tag{19}$$

where f, g, and Π are arbitrary twice continuously differentiable, continuously differentiable, and continuous functions, respectively; the unit vectors $\mathbf{g}$ and $\mathbf{d}$ represent polarization vectors of mechanical and electrical displacements, respectively; the unit vector $\mathbf{n}$ denotes the direction of wave propagation; and c is the phase velocity of the wave.

Substitution of Eqs. (17) and (19) into Eqs. (12) and (18) yields

$$\hat{\mathbf{A}}\cdot\mathbf{g} = \rho c^2\mathbf{g} \quad \text{and} \quad \mathbf{g}\cdot\mathbf{n} = 0 \tag{20}$$

where $\hat{\mathbf{A}}$ is the so-called generalized acoustic tensor defining the condition of propagation of plane elastic waves in an incompressible electroelastic solid. The generalized acoustic tensor for an electroelastic material with an arbitrary energy potential $\psi(\mathbf{F}, \mathbf{D}_L)$ can be calculated as follows [37]:

$$\hat{\mathbf{A}} = \hat{\mathbf{Q}} - \frac{2}{(\mathrm{tr}\hat{\mathbf{K}})^2 - \mathrm{tr}\hat{\mathbf{K}}^2}\hat{\mathbf{R}}\cdot((\mathrm{tr}\hat{\mathbf{K}})\hat{\mathbf{I}} - \hat{\mathbf{K}})\cdot\hat{\mathbf{R}}^{T} \tag{21}$$

where

$$\hat{\mathbf{I}} = \mathbf{I} - \mathbf{n}\otimes\mathbf{n} \tag{22}$$

is the projection on the plane normal to $\mathbf{n}$; $\hat{\mathbf{K}} = \hat{\mathbf{I}}\cdot\mathbf{K}\cdot\hat{\mathbf{I}}$, $\hat{\mathbf{Q}} = \hat{\mathbf{I}}\cdot\mathbf{Q}\cdot\hat{\mathbf{I}}$ and $\hat{\mathbf{R}} = \hat{\mathbf{I}}\cdot\mathbf{R}\cdot\hat{\mathbf{I}}$, where

$$Q_{ik} = \mathbb{C}_{ijkl}n_jn_l \quad \text{and} \quad \mathbf{R} = \mathbf{n}\cdot\boldsymbol{\mathcal{M}} \tag{23}$$

Note that the generalized acoustic tensor $\hat{\mathbf{A}}$ is symmetric. Recall that an incompressible electroelastic material is strongly elliptic (stable), if its generalized acoustic tensor $\hat{\mathbf{A}}$ is positively defined, i.e., $\mathbf{g}\cdot\hat{\mathbf{A}}\cdot\mathbf{g} > 0$ for any unit vectors $\mathbf{n}$ and $\mathbf{g}$ satisfying the incompressibility constraint $(J = 1)$ $\mathbf{n}\cdot\mathbf{g} = 0$ along an electromechanical loading path defined through a combination of $\mathbf{D}_L$ and $\mathbf{F}$.

3 Analysis and Results

Consider periodic laminates made out of two isotropic incompressible alternating ideal DE phases with volume fractions $v^{(a)}$ and $v^{(b)} = 1 - v^{(a)}$. Here and thereafter, the fields and parameters of the phases are denoted by superscripts $(\bullet)^{(a)}$ and $(\bullet)^{(b)}$, respectively. Geometrically, the layers are characterized by their thicknesses $H^{(a)} = v^{(a)}H$ and $H^{(b)} = v^{(b)}H$, where H is the period of the undeformed laminate (see Fig. 1(*a*)). In the deformed laminates (see Fig. 1(*b*)), the layer thicknesses change as follows:

$$h^{(a)} = \lambda_2^{(a)}H^{(a)}, \quad h^{(b)} = \lambda_2^{(b)}H^{(b)}, \text{ and } h = \bar{\lambda}_2 H \tag{24}$$

where $\bar{\lambda}_2 = v^{(a)}\lambda_2^{(a)} + v^{(b)}\lambda_2^{(b)}$ and $\lambda_2^{(a,b)}$ are the stretch ratios in the direction $\mathbf{e}_2$ for phases a and b, respectively.

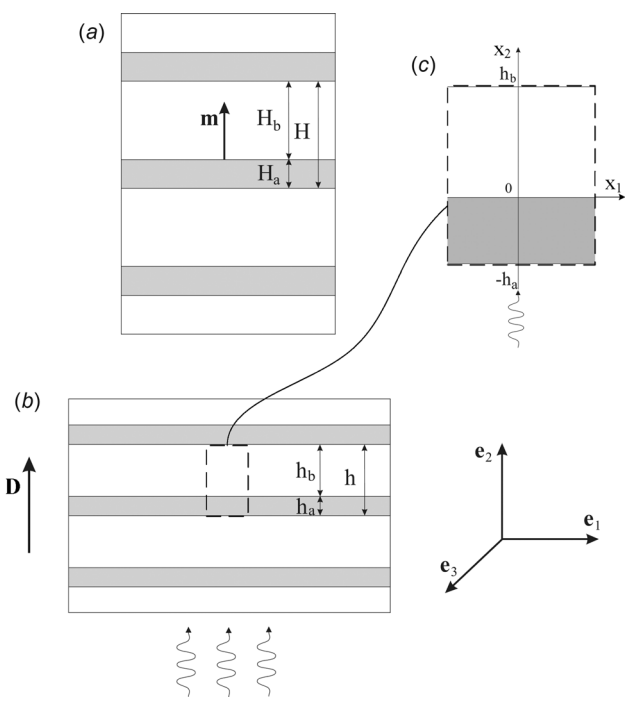

Fig. 1 Schematic representation of the undeformed (*a*) and subjected to the electromechanical load (*b*) periodic layered material with alternating phases *a* and *b*. A unit cell (*c*); $(\mathbf{e}_1, \mathbf{e}_2, \mathbf{e}_3)$ is the orthonormal basis.

The macroscopically applied electromechanical loads are expressed in terms of the average deformation gradient $\bar{\mathbf{F}}$ and Lagrangian electric displacement $\bar{\mathbf{D}}_L$, namely

$$\bar{\mathbf{F}} = v^{(a)}\mathbf{F}^{(a)} + v^{(b)}\mathbf{F}^{(b)} \quad \text{and} \quad \bar{\mathbf{D}}_L = v^{(a)}\mathbf{D}_L^{(a)} + v^{(b)}\mathbf{D}_L^{(b)} \tag{25}$$

The continuity of the displacements along the interface between the layers yields condition for the deformation gradients $\mathbf{F}^{(a)}$ and $\mathbf{F}^{(b)}$

$$(\mathbf{F}^{(a)} - \mathbf{F}^{(b)}) \cdot \mathbf{q} = \mathbf{0} \tag{26}$$

and the continuity of the tractions across the interface between the layers yields

$$(\mathbf{P}^{(a)} - \mathbf{P}^{(b)}) \cdot \mathbf{m} = \mathbf{0} \tag{27}$$

where unit vector $\mathbf{m}$ denotes the initial lamination direction (see Fig. 1(*a*)), and $\mathbf{q}$ is an arbitrary unit vector perpendicular to $\mathbf{m}$. In the absence of free charges at the interfaces, the jump conditions for Lagrangian electric displacement and electric field are

$$(\mathbf{D}_L^{(a)} - \mathbf{D}_L^{(b)}) \cdot \mathbf{m} = 0 \quad \text{and} \quad (\mathbf{E}_L^{(a)} - \mathbf{E}_L^{(b)}) \times \mathbf{m} = \mathbf{0} \tag{28}$$

In the current configuration, the interface jump conditions (27) and (28) read as

$$(\boldsymbol{\tau}^{(a)} - \boldsymbol{\tau}^{(b)}) \cdot \mathbf{m} = \mathbf{0}, \quad (\mathbf{D}^{(a)} - \mathbf{D}^{(b)}) \cdot \mathbf{m} = 0 \quad \text{and} \quad (\mathbf{E}^{(a)} - \mathbf{E}^{(b)}) \times \mathbf{m} = \mathbf{0} \tag{29}$$

3.1 Long Wave Estimates for DE Laminates Under Electromechanical Loads. Let us consider DE laminates with isotropic *incompressible* dielectric phases described by the neo-Hookean ideal dielectric model, namely

$$\psi^{(\xi)} = \frac{\mu^{(\xi)}}{2}(\mathbf{F}^{(\xi)} : \mathbf{F}^{(\xi)} - 3) + \frac{1}{2\varepsilon^{(\xi)}}\mathbf{D}_L^{(\xi)} \cdot \mathbf{C}^{(\xi)} \cdot \mathbf{D}_L^{(\xi)} \tag{30}$$

where $\mu^{(\xi)}$ and $\varepsilon^{(\xi)}$ are the shear modulus and the electric permittivity in the undeformed state, respectively; $\mathbf{C} = \mathbf{F}^T \cdot \mathbf{F}$ is the right Cauchy–Green tensor. Under the incompressibility assumption, a closed-form exact solution for finitely deformed periodic layered electroactive materials with neo-Hookean ideal dielectric phases can be derived [21,24–26]. By utilizing the exact analytical solution, an effective free energy function can be constructed [37]

$$\psi(\bar{\mathbf{F}}, \bar{\mathbf{D}}_L) = \frac{\bar{\mu}}{2}(\bar{\mathbf{F}} : \bar{\mathbf{F}} - 3) - \frac{\bar{\mu} - \breve{\mu}}{2}\left(\mathbf{m} \cdot \bar{\mathbf{C}} \cdot \mathbf{m} - \frac{1}{\mathbf{m} \cdot \bar{\mathbf{C}}^{-1} \cdot \mathbf{m}}\right) + \frac{1}{2\bar{\varepsilon}}\bar{\mathbf{D}}_L \cdot \bar{\mathbf{C}} \cdot \bar{\mathbf{D}}_L + \frac{1}{2}\left(\frac{1}{\breve{\varepsilon}} - \frac{1}{\bar{\varepsilon}}\right)\frac{(\bar{\mathbf{D}}_L \cdot \mathbf{m})^2}{\mathbf{m} \cdot \bar{\mathbf{C}}^{-1} \cdot \mathbf{m}} \tag{31}$$

where $\bar{\mathbf{C}} = \bar{\mathbf{F}}^T \cdot \bar{\mathbf{F}}$ is the average right Cauchy–Green tensor, and

$$\bar{\mu} = v^{(a)}\mu^{(a)} + v^{(b)}\mu^{(b)} \quad \text{and} \quad \breve{\mu} = \left(\frac{v^{(a)}}{\mu^{(a)}} + \frac{v^{(b)}}{\mu^{(b)}}\right)^{-1} \tag{32}$$

$$\bar{\varepsilon} = v^{(a)}\varepsilon^{(a)} + v^{(b)}\varepsilon^{(b)} \quad \text{and} \quad \breve{\varepsilon} = \left(\frac{v^{(a)}}{\varepsilon^{(a)}} + \frac{v^{(b)}}{\varepsilon^{(b)}}\right)^{-1} \tag{33}$$

The generalized acoustic tensor (21) corresponding to the free energy function (31) takes the form

$$\hat{\mathbf{A}}(\mathbf{n}, \bar{\mathbf{F}}, \bar{\mathbf{D}}_L) = A_1\hat{\mathbf{I}} + A_2(\hat{\mathbf{I}} \cdot \bar{\mathbf{F}}^{-T} \cdot \mathbf{m}) \otimes (\hat{\mathbf{I}} \cdot \bar{\mathbf{F}}^{-T} \cdot \mathbf{m}) \tag{34}$$

where

$$A_1 = \bar{\mu}(\mathbf{n} \cdot \bar{\mathbf{B}} \cdot \mathbf{n}) + (\breve{\mu} - \bar{\mu})(\mathbf{n} \cdot \bar{\mathbf{F}} \cdot \mathbf{m})^2 \tag{35}$$

and

$$A_2 = \frac{\bar{\mu} - \breve{\mu}}{\alpha^2}\left(\frac{4\beta^2}{\alpha} - 1\right) - \left(\frac{1}{\breve{\varepsilon}} - \frac{1}{\bar{\varepsilon}}\right) \times \left(\frac{(\bar{\mathbf{D}}_L \cdot \mathbf{m})^2}{\alpha^2} - \frac{4}{\gamma}\left(\frac{(\bar{\mathbf{D}}_L \cdot \mathbf{m})^2\beta^2}{\alpha^2} + \frac{1}{4}(\mathbf{n} \cdot \bar{\mathbf{F}} \cdot \bar{\mathbf{D}}_L)^2 - \frac{(\bar{\mathbf{D}}_L \cdot \mathbf{m})(\mathbf{n} \cdot \bar{\mathbf{F}} \cdot \bar{\mathbf{D}}_L)\beta}{\alpha}\right)\right) \tag{36}$$

where $\bar{\mathbf{B}} = \bar{\mathbf{F}} \cdot \bar{\mathbf{F}}^T$ is the average left Cauchy–Green tensor, $\alpha = \mathbf{m} \cdot \bar{\mathbf{C}}^{-1} \cdot \mathbf{m}$, $\beta = \mathbf{n} \cdot \bar{\mathbf{F}}^{-T} \cdot \mathbf{m}$, and $\gamma = \alpha\bar{\varepsilon}/\breve{\varepsilon} + \beta^2(1 - \bar{\varepsilon}/\breve{\varepsilon})$. One can show that the generalized acoustic tensor (34) has the following eigenvalues in the two-dimensional space normal to $\mathbf{n}$:

$$a_1 = A_1 \quad \text{and} \quad a_2 = A_1 + A_2(\alpha - \beta^2) \tag{37}$$

In general, we have two distinct shear waves propagating in finitely deformed DE laminates in the presence of an electric field. The corresponding phase velocities are

$$\bar{c}_{\text{sw}}^{(1)} = \sqrt{a_1/\bar{\rho}} \quad \text{and} \quad \bar{c}_{\text{sw}}^{(2)} = \sqrt{a_2/\bar{\rho}} \tag{38}$$

where $\bar{\rho} = v^{(a)}\rho^{(a)} + v^{(b)}\rho^{(b)}$ is the average density of the laminate. Remarkably, the first shear wave phase velocity $\bar{c}_{\text{sw}}^{(1)}$ is explicitly independent of the electric field; moreover, it coincides with the phase velocity of the corresponding shear wave propagating in finitely deformed laminate in the absence of an electric field [36]. However, the second shear wave phase velocity $\bar{c}_{\text{sw}}^{(2)}$ depends explicitly on electric field.

Let us consider some particular cases, where for simplicity, we set

$$\mathbf{m} = \mathbf{e}_2 \quad \text{and} \quad \bar{\mathbf{F}} = \bar{\lambda}_1\mathbf{e}_1 \otimes \mathbf{e}_1 + \bar{\lambda}_2\mathbf{e}_2 \otimes \mathbf{e}_2 + \bar{\lambda}_3\mathbf{e}_3 \otimes \mathbf{e}_3 \tag{39}$$

First, we study shear waves propagating perpendicular to layers, i.e., $\mathbf{n} = \mathbf{e}_2$. Regardless of the value and the direction of the applied electric displacement, the phase velocities of both shear waves are identical and independent of electric quantities, namely

$$\bar{c}_{\text{sw}} = \bar{c}_{\text{sw}}^{(1)} = \bar{c}_{\text{sw}}^{(2)} = \bar{\lambda}_2\sqrt{\breve{\mu}/\bar{\rho}} \tag{40}$$

Thus, the phase velocities (40) depend on electric field only if $\bar{\lambda}_2 = \bar{\lambda}_2(\bar{\mathbf{D}}_L)$.

Second, we apply an electric field along the layers, $\bar{\mathbf{D}}_L = \bar{D}_L\sqrt{\bar{\mu}\breve{\varepsilon}}\,\mathbf{e}_1$, and study shear waves propagating along the layers. Thus, for wave propagation in the same direction as the applied electric field ($\mathbf{n} = \mathbf{e}_1$), the phase velocities of the shear waves are distinct, and one of them depends on the electric field, namely

$$\bar{c}_{\text{sw}}^{(1)} = \bar{\lambda}_1\sqrt{\bar{\mu}/\bar{\rho}} \quad (\mathbf{g}^{(1)} = \mathbf{e}_3) \tag{41}$$

and

$$\bar{c}_{\text{sw}}^{(2)} = \sqrt{\left(\bar{\lambda}_2^2\left(\frac{\bar{\mu}}{\breve{\mu}} - 1\right) + \bar{\lambda}_1^2\left(1 + \bar{D}_L^2\frac{\breve{\varepsilon}}{\bar{\varepsilon}}\left(1 - \frac{\breve{\varepsilon}}{\bar{\varepsilon}}\right)\right)\right)\frac{\bar{\mu}}{\bar{\rho}}} \quad (\mathbf{g}^{(2)} = \mathbf{e}_2) \tag{42}$$

However, for wave propagation perpendicular to the electric field ($\mathbf{n} = \mathbf{e}_3$), the phase velocities of the shear waves are distinct and independent of electric field, namely

$$\bar{c}_{\mathrm{sw}}^{(1)} = \bar{\lambda}_3 \sqrt{\bar{\mu}/\bar{\rho}} \quad (\mathbf{g}^{(1)} = \mathbf{e}_1) \tag{43}$$

and

$$\bar{c}_{\mathrm{sw}}^{(2)} = \sqrt{\left(\bar{\lambda}_2^2\left(\frac{\breve{\mu}}{\bar{\mu}} - 1\right) + \bar{\lambda}_3^2\right)\frac{\bar{\mu}}{\bar{\rho}}} \quad \left(\mathbf{g}^{(2)} = \mathbf{e}_2\right) \tag{44}$$

Third, we apply an electric field perpendicular to the layers ($\bar{\mathbf{D}}_L = D_L\sqrt{\bar{\mu}\breve{\varepsilon}}\,\mathbf{e}_2$) and analyze shear wave propagation along the layers ($\mathbf{n} = \mathbf{e}_{1,3}$). In this case, the phase velocities of shear waves are different, and the phase velocity of the so-called in-plane shear wave (with polarization $\mathbf{g}^{(2)} = \mathbf{e}_2$) depends explicitly on electric field, i.e.,

$$\bar{c}_{\mathrm{sw}}^{(1)} = \bar{\lambda}_{1,3} \sqrt{\bar{\mu}/\bar{\rho}} \quad (\mathbf{g}^{(1)} = \mathbf{e}_{3,1}) \tag{45}$$

and

$$\bar{c}_{\mathrm{sw}}^{(2)} = \sqrt{\left(\bar{\lambda}_{1,3}^2 + \bar{\lambda}_2^2\left(\frac{\breve{\mu}}{\bar{\mu}} - 1 - D_L^2\left(1 - \frac{\breve{\varepsilon}}{\bar{\varepsilon}}\right)\right)\right)\frac{\bar{\mu}}{\bar{\rho}}} \quad \left(\mathbf{g}^{(2)} = \mathbf{e}_2\right) \tag{46}$$

Now, let us consider the example when deformation of DE laminates is induced by an electric field applied perpendicular to the layers, i.e.,

$$\begin{aligned} &\mathbf{m} = \mathbf{e}_2, \quad \bar{\mathbf{D}}_L = D_L\sqrt{\bar{\mu}\breve{\varepsilon}}\,\mathbf{e}_2, \ \text{and} \\ &\bar{\boldsymbol{\tau}} = v^{(a)}\boldsymbol{\tau}^{(a)} + v^{(b)}\boldsymbol{\tau}^{(b)} = \mathbf{0} \end{aligned} \tag{47}$$

Then, the symmetry of the problem in the plane $\langle \mathbf{e}_1, \mathbf{e}_3 \rangle$, the incompressibility assumption, and the continuity condition for displacements along interfaces between the layers (26) yield the average deformation gradient in the form

$$\bar{\mathbf{F}} = \lambda \mathbf{e}_2 \otimes \mathbf{e}_2 + \lambda^{-1/2}(\mathbf{I} - \mathbf{e}_2 \otimes \mathbf{e}_2) \tag{48}$$

The total Cauchy stress and electric field within each phase are

$$\boldsymbol{\tau}^{(\xi)} = \mu^{(\xi)}\mathbf{B}^{(\xi)} + (\varepsilon^{(\xi)})^{-1}\mathbf{D}^{(\xi)} \otimes \mathbf{D}^{(\xi)} - p^{(\xi)}\mathbf{I} \ \text{and} \ \mathbf{E}^{(\xi)} = \mathbf{D}^{(\xi)}/\varepsilon^{(\xi)} \tag{49}$$

where in our case, $\mathbf{D}^{(\xi)} = D_2\mathbf{e}_2 = \lambda D_L\sqrt{\bar{\mu}\breve{\varepsilon}}\,\mathbf{e}_2$ and $\mathbf{B}^{(\xi)} = \lambda^2\mathbf{e}_2 \otimes \mathbf{e}_2 + \lambda^{-1}(\mathbf{I} - \mathbf{e}_2 \otimes \mathbf{e}_2)$. Hence

$$\begin{aligned} &\tau_{11}^{(\xi)} = \tau_{33}^{(\xi)} = \mu^{(\xi)}\lambda^{-1} - p^{(\xi)} \ \text{and} \\ &\tau_{22}^{(\xi)} = \mu^{(\xi)}\lambda^2 + (\varepsilon^{(\xi)})^{-1}\bar{\mu}\breve{\varepsilon}\,\lambda^2 D_L^2 - p^{(\xi)} \end{aligned} \tag{50}$$

The continuity condition $(29)_1$ and $(47)_3$ yield

$$\tau_{22}^{(a)} = \tau_{22}^{(b)} = 0 \ \text{and} \ v^{(a)}\tau_{11}^{(a)} + v^{(b)}\tau_{11}^{(b)} = 0 \tag{51}$$

By solving the system of equations (51), we obtain an expression for the induced stretch

$$\lambda = (1 + D_L^2)^{-1/3} \tag{52}$$

In terms of the Lagrangian electric field

$$\bar{\mathbf{E}}_L = E_L\sqrt{\frac{\bar{\mu}}{\breve{\varepsilon}}}\mathbf{e}_2 \tag{53}$$

where $E_L = \lambda^2 D_L$. Equation (52) reads as

$$E_L^2 = \lambda(1 - \lambda^3) \tag{54}$$

Equation (54) yields only one physically relevant solution, namely

$$\lambda = \left(1 + \sqrt{12\eta^{-3} - 1}\right)\frac{\eta}{2\sqrt[3]{6}} \tag{55}$$

where

$$\eta = \sqrt{\frac{8\sqrt[3]{3}\mathrm{E}_\mathrm{L}^2}{\sqrt[3]{9 + \sqrt{3(27 - 256E_L^6)}}} + \sqrt[3]{2\left(9 + \sqrt{3(27 - 256E_L^6)}\right)}} \tag{56}$$

Note that Eq. (54) yields expressions for the so-called limiting electric field and the corresponding stretch induced by this field, namely

$$\begin{aligned} &E_L^{\lim} = \frac{\sqrt{3}}{2\sqrt[3]{2}} \simeq 0.687, \quad \lambda^{\lim} = 2^{-2/3} \simeq 0.63, \ \text{and} \\ &D_L^{\lim} = \sqrt{3} \simeq 1.732 \end{aligned} \tag{57}$$

Figure 2(*a*) shows the induced stretch (55) as the function of the dimensionless Lagrangian electric field. Remarkably, the limiting

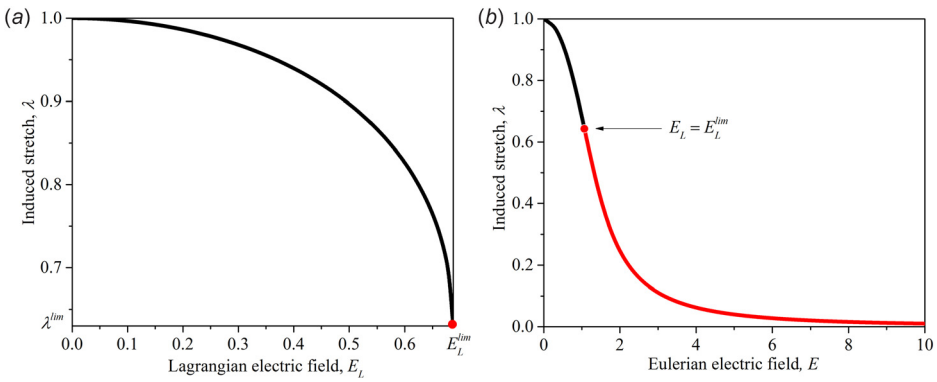

Fig. 2 Induced stretch as function of dimensionless Lagrangian (*a*) and Eulerian (*b*) electric fields

induced stretch $\lambda_{\lim} = 2^{-2/3}$ does not depend on composition of the laminate and coincides with the limiting stretch for homogeneous DEs [38]. The induced stretch can be expressed as a function of the Eulerian electric field, $\bar{\mathbf{E}} = \bar{\mathbf{F}}^{-T} \cdot \bar{\mathbf{E}}_L = E\sqrt{\bar{\mu}/\breve{\varepsilon}}\,\mathbf{e}_2$, where $E = \lambda^{-1}E_L$. Thus, Eq. (54) reads as

$$E^2 = \lambda^{-1} - \lambda^2 \tag{58}$$

Figure 2(*b*) shows the induced stretch as the function of the normalized true or Eulerian electric field as described by Eq. (58). Analogously to the case of homogeneous DEs [38], the limiting value of electric field may be interpreted as the starting point of thinning down without limit, after the critical value of electric field is reached, $E \geq E^{\lim} = 2^{-2/3}\sqrt{3}$. Hence, in the continuation, we present our examples for electric fields ranging from 0 up to $E^{\lim}$.

For the considered electrostatically induced deformations (48) and (52), the expressions for the phase velocities (40), (45), and (46) read as

(1) $\mathbf{n} = \mathbf{e}_2$

$$\bar{c}_{\mathrm{sw}} = \bar{c}_{\mathrm{sw}}^{(1)} = \bar{c}_{\mathrm{sw}}^{(2)} = (1 + D_L^2)^{-1/3}\sqrt{\breve{\mu}/\bar{\rho}} \tag{59}$$

(2) $\mathbf{n} = \mathbf{e}_{1,3}$

$$\bar{c}_{\mathrm{sw}}^{(1)} = (1 + D_L^2)^{1/6}\sqrt{\bar{\mu}/\bar{\rho}} \quad (\mathbf{g}^{(1)} = \mathbf{e}_{3,1}) \tag{60}$$

and

$$\bar{c}_{\mathrm{sw}}^{(2)} = \left(1 + D_L^2\right)^{-1/3}\sqrt{\left(1 + D_L^2\frac{\breve{\varepsilon}}{\bar{\varepsilon}}\frac{\bar{\mu}}{\breve{\mu}}\right)\frac{\breve{\mu}}{\bar{\rho}}} \quad \left(\mathbf{g}^{(2)} = \mathbf{e}_2\right) \tag{61}$$

Note that if $\mu^{(a)}/\mu^{(b)} = \varepsilon^{(a)}/\varepsilon^{(b)}$, then $\breve{\varepsilon}/\bar{\varepsilon} = \breve{\mu}/\bar{\mu}$; hence, for $\mu^{(a)}/\mu^{(b)} = \varepsilon^{(a)}/\varepsilon^{(b)}$, Eq. (61) reduces to

$$\bar{c}_{\mathrm{sw}}^{(2)} = (1 + D_L^2)^{1/6}\sqrt{\breve{\mu}/\bar{\rho}} \quad (\mathbf{g}^{(2)} = \mathbf{e}_2) \tag{62}$$

Figure 3 shows the normalized phase velocities of the shear waves (59)–(61) as functions of the dimensionless Lagrangian electric displacement. We normalize the phase velocities by the corresponding values in the absence of an electric field, i.e., $\bar{c}_0 = \bar{c}_{\mathrm{sw}}|_{D_L=0}$; therefore, all presented curves are valid for any density contrasts $\rho^{(a)}/\rho^{(b)}$ between the layers; moreover, thanks to the normalization the dash-dotted gray curve, corresponding to the wave propagating perpendicular to the layers, is valid for any composition of DE laminates. The phase velocities of both shear waves propagating perpendicular to the layers coincide and monotonically decrease with an increase in electric displacement; in particular, the phase velocities decrease by ~37 % for $D = D_{\lim}$ (see the dash-dotted gray curve in Fig. 3).

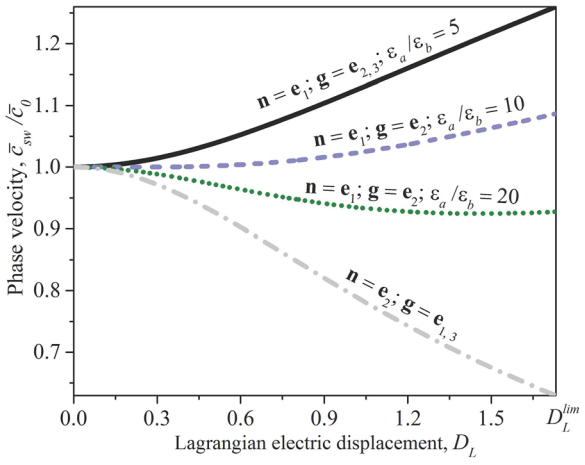

Fig. 3 The phase velocities of shear waves (59)–(61) as functions of the dimensionless electric displacement for laminates with $\nu^{(a)} = 0.2$ and $\mu^{(a)}/\mu^{(b)} = 5$. The phase velocities are normalized by the corresponding values in the absence of electric field.

To illustrate the influence of electric field and direction of wave propagation on the characteristics of elastic waves in the layered DEs, we consider wave propagation in the plane $\langle \mathbf{e}_1, \mathbf{e}_2 \rangle$, i.e., $\mathbf{n} = \cos\varphi\,\mathbf{e}_1 + \sin\varphi\,\mathbf{e}_2$. Thus, the expression for the phase velocities (38) together with Eqs. (48) and (52) reduces to

$$\bar{c}_{\mathrm{sw}}^{(1)}(\varphi) = \left(1 + D_L^2\right)^{-1/3}\sqrt{\left(\left(1 + D_L^2\right)\cos^2\varphi + \frac{\breve{\mu}}{\bar{\mu}}\sin^2\varphi\right)\frac{\bar{\mu}}{\bar{\rho}}} \tag{63}$$

and

$$\bar{c}_{\mathrm{sw}}^{(2)}(\varphi) = \left(1 + D_L^2\right)^{-1/3} \times \sqrt{\left(\frac{\breve{\mu}}{\bar{\mu}}\cos^2 2\varphi + \sin^2 2\varphi + D_L^2\cos^2\varphi\left(\frac{\bar{\varepsilon}}{\breve{\varepsilon}}\cos^2\varphi + \sin^2\varphi\right)^{-1}\right)\frac{\bar{\mu}}{\bar{\rho}}} \tag{64}$$

By making use of the explicit relations (63) and (64), we construct the polar diagrams of slownesses $\bar{s}_{\mathrm{sw}}(\varphi) = 1/\bar{c}_{\mathrm{sw}}(\varphi)$. Figure 4 shows an example of the slowness curves for the so-called out-of-plane (with polarization $\mathbf{g} = \mathbf{e}_3$) and in-plane (with polarization lying in the plane $\langle \mathbf{e}_1, \mathbf{e}_2 \rangle$) shear waves in the DE laminates subjected to an electric field applied perpendicular to the layers. Remarkably, the slownesses of the in-plane shear waves increase for any direction of wave propagation in DE laminates subjected to an electric field, if contrast in electric permittivities is larger than the contrast in shear moduli (see Fig. 4(*d*)).

The dispersion relations for long waves in the incompressible DE laminates are derived from Eq. (38), and have the following form:

$$\bar{\omega}_{\mathrm{sw}}^{(1)} = \sqrt{b_1/\bar{\rho}} \quad \text{and} \quad \bar{\omega}_{\mathrm{sw}}^{(2)} = \sqrt{b_2/\bar{\rho}} \tag{65}$$

where

$$b_1 = \bar{\mu}(\mathbf{k}\cdot\bar{\mathbf{B}}\cdot\mathbf{k}) + (\breve{\mu} - \bar{\mu})(\mathbf{k}\cdot\bar{\mathbf{F}}\cdot\mathbf{m})^2 \tag{66}$$

and

$$b_2 = b_1 + \left(\alpha k^2 - \beta_k^2\right)\left[\frac{\bar{\mu} - \breve{\mu}}{\alpha^2}\left(\frac{4\beta_k^2}{\alpha k^2} - 1\right) - \left(\frac{1}{\breve{\varepsilon}} - \frac{1}{\bar{\varepsilon}}\right) \times \left(\frac{(\bar{\mathbf{D}}_L\cdot\mathbf{m})^2}{\alpha^2} - \frac{4}{\gamma_k}\left(\frac{(\bar{\mathbf{D}}_L\cdot\mathbf{m})^2\beta_k^2}{\alpha^2} + \frac{1}{4}(\mathbf{k}\cdot\bar{\mathbf{F}}\cdot\bar{\mathbf{D}}_L)^2 - \frac{(\bar{\mathbf{D}}_L\cdot\mathbf{m})(\mathbf{k}\cdot\bar{\mathbf{F}}\cdot\bar{\mathbf{D}}_L)\beta_k}{\alpha}\right)\right)\right] \tag{67}$$

where $\mathbf{k}$ is the wave vector, $k = |\mathbf{k}|$ is the wave number, $\beta_k = \mathbf{k}\cdot\bar{\mathbf{F}}^{-T}\cdot\mathbf{m}$ and $\gamma_k = \alpha k^2\bar{\varepsilon}/\breve{\varepsilon} + \beta_k^2(1 - \bar{\varepsilon}/\breve{\varepsilon})$.

Now, group velocity can be calculated as

$$\mathbf{v}_g = \nabla_{\mathbf{k}}\bar{\omega} \tag{68}$$

From Eqs. (65) and (68), we obtain the explicit formulae for the shear wave group velocities in homogenized DE laminates

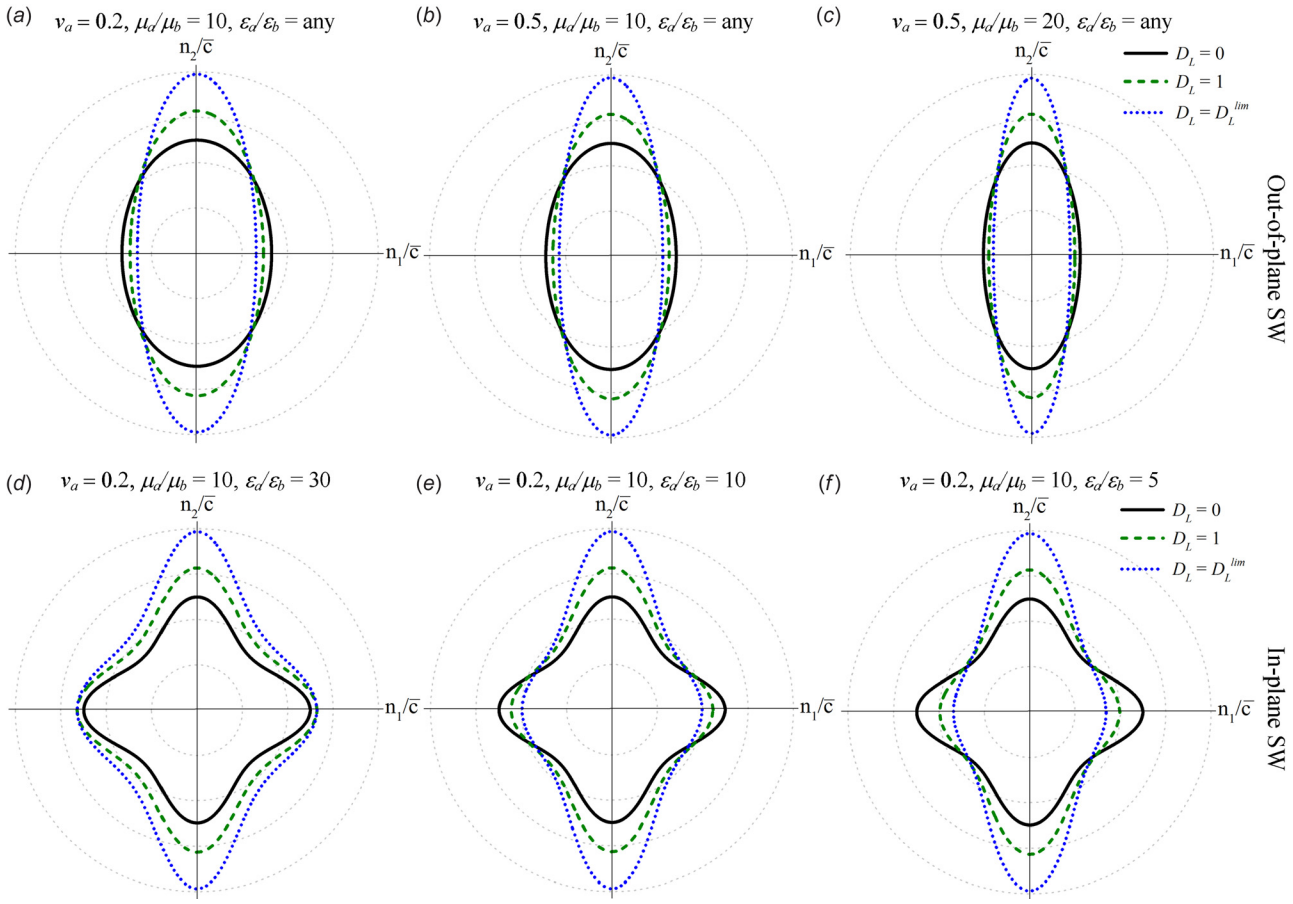

Fig. 4 Slowness curves for the out-of-plane (*a*)–(*c*) and in-plane (*d*)–(*f*) shear waves propagating in the DE laminates with different compositions subjected to electric field perpendicular to the layers. Scale is 0.4 per division, and slowness is normalized by $\sqrt{\bar{\mu}/\bar{\rho}}$. Note that the horizontal and vertical axes with the corresponding labels $n_1/\bar{c}$ and $n_2/\bar{c}$ serve for showing the principal directions and physical quantity presented on the polar plot only.

$$\mathbf{v}_{\mathrm{sw}}^{(1)} = \frac{\bar{\mu}\bar{\mathbf{B}}\cdot\mathbf{n} + (\breve{\mu} - \bar{\mu})(\mathbf{n}\cdot\bar{\mathbf{F}}\cdot\mathbf{m})\bar{\mathbf{F}}\cdot\mathbf{m}}{\sqrt{\bar{\rho}a_1}} \tag{69}$$

and

$$\begin{aligned}\mathbf{v}_{\mathrm{sw}}^{(2)} = {} & \frac{1}{\sqrt{\bar{\rho}a_2}}\left(\bar{\mu}\bar{\mathbf{B}}\cdot\mathbf{n} + (\breve{\mu} - \bar{\mu})(\mathbf{n}\cdot\bar{\mathbf{F}}\cdot\mathbf{m})\bar{\mathbf{F}}\cdot\mathbf{m}\right. \\ & + \frac{\bar{\mu}-\breve{\mu}}{\alpha^2}\left(\beta\left(5 - \frac{8\beta^2}{\alpha}\right)\bar{\mathbf{F}}^{-T}\cdot\mathbf{m} + \left(\frac{4\beta^4}{\alpha} - \alpha\right)\mathbf{n}\right) \\ & + \left(\frac{1}{\breve{\varepsilon}} - \frac{1}{\bar{\varepsilon}}\right)\left\{\frac{D_m^2}{\alpha^2}\left(\beta\bar{\mathbf{F}}^{-T}\cdot\mathbf{m} - \alpha\mathbf{n}\right)\right. \\ & + \frac{2}{\gamma^2}\left[2\beta^2\left(\beta D_m\left(\frac{\beta D_m}{\alpha} - F_{nD}\right) + \frac{\alpha}{4}F_{nD}^2\right)\mathbf{n}\right. \\ & + \gamma(\alpha-\beta^2)\left(\frac{1}{2}F_{nD} - \frac{D_m\beta}{\alpha}\right)\bar{\mathbf{F}}\cdot\bar{\mathbf{D}}_L \\ & + \left(\beta\left(D_m\beta\left(\frac{\beta^2}{\alpha}\left(F_{nD} - \frac{2D_m\beta}{\alpha}\right) + F_{nD}\right) - \frac{\alpha}{2}F_{nD}^2\right)\right. \\ & + \frac{\bar{\varepsilon}D_m}{\breve{\varepsilon}}\left(2D_m\beta\left(1 - \frac{2\beta^2}{\alpha}\right) + F_{nD}(2\beta^2 - \alpha)\right. \\ & \left.\left.\left.\left.\left. - \frac{\beta^4}{\alpha}\left(F_{nD} - \frac{2D_m\beta}{\alpha}\right)\right)\right)\bar{\mathbf{F}}^{-T}\cdot\mathbf{m}\right]\right\}\Bigg)\end{aligned} \tag{70}$$

where $D_m = \bar{\mathbf{D}}_L\cdot\mathbf{m}$ and $F_{nD} = \mathbf{n}\cdot\bar{\mathbf{F}}\cdot\bar{\mathbf{D}}_L$. We note that, for $\mathbf{m} = \mathbf{e}_2$ and $\bar{\mathbf{F}} = \bar{\lambda}_1\mathbf{e}_1\otimes\mathbf{e}_1 + \bar{\lambda}_2\mathbf{e}_2\otimes\mathbf{e}_2 + \bar{\lambda}_3\mathbf{e}_3\otimes\mathbf{e}_3$, the absolute values of the group velocities coincide with the phase velocities for the waves propagating along the principal directions in the DE laminates subjected to the electric field along or perpendicular to the layers.

To illustrate the influence of electric field and direction of wave propagation on the energy propagation in DE laminates, we consider wave propagation in the plane $\langle\mathbf{e}_1,\mathbf{e}_2\rangle$, i.e., $\mathbf{n} = \cos\varphi\,\mathbf{e}_1 + \sin\varphi\,\mathbf{e}_2$. Recall that the outer normal to the slowness curve defines the direction of the energy flow [39]. Thus, by assigning the absolute value of the group velocity (i.e., $|\mathbf{v}_{\mathrm{sw}}|$) to the normal to the slowness curve for all possible propagation directions, we construct the polar diagrams for the group velocity or the energy curves [39,40]. In particular, the expression for the group velocities (69) and (70) together with Eqs. (48) and (52) yields energy curves shown in Fig. 5. Clearly, the group velocities of shear waves (SWs) strongly depend on the propagation direction and applied electric field. Application of electric field perpendicular to the layers increases the group velocity of the out-of-plane SW propagating along the layers and decreases it for SW propagating perpendicular to the layers regardless of laminate composition (see Figs. 5(*a*)–5(*c*)). While the group velocity of the in-plane SW propagating along the layers can either decrease or increase with application of electric field depending on the laminate composition (compare Figs. 5(*d*)–5(*f*)). Moreover, the energy curves of the in-plane SWs have intersections, meaning that the absolute values and directions of the group velocities coincide for two distinct wave propagation directions. Remarkably, the position of these

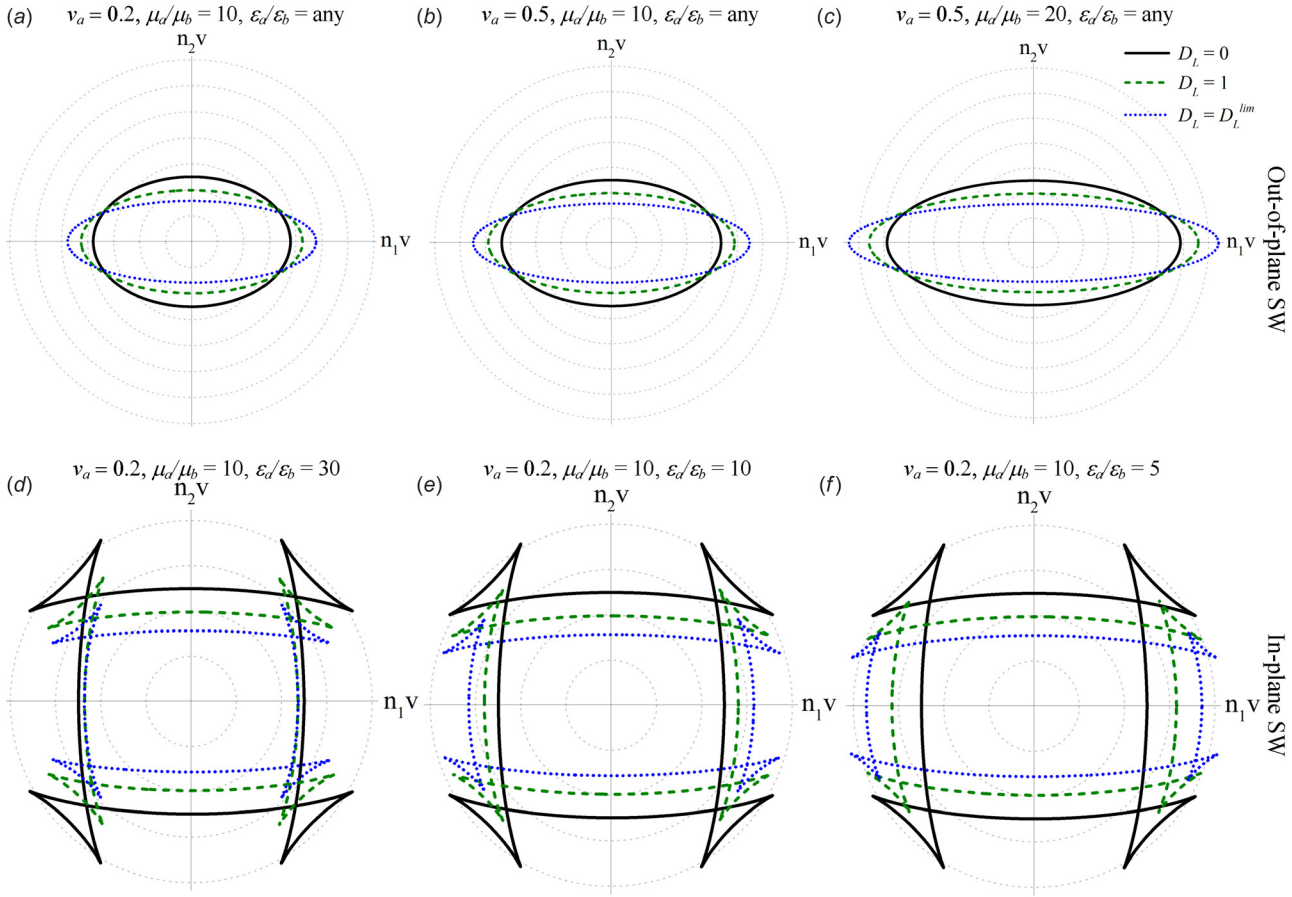

Fig. 5 Energy curves for the out-of-plane (*a*)–(*c*) and in-plane (*d*)–(*f*) shear waves propagating in the DE laminates with different compositions subjected to electric field perpendicular to the layers. Scale is 0.4 per division, where group velocity is normalized by $\sqrt{\bar{\rho}}/\bar{\mu}$. Note that the horizontal and vertical lines with the corresponding labels ($n_1 v$) and ($n_2 v$) serve for showing the principal directions and physical quantity presented on the polar plot only.

intersections changes with a change in the magnitude of the applied electric field. It is worth noting also that the energy curves of plane waves presented here may serve as a tool to define the wave fronts of impulsive point source excited waves in homogenized laminates [40,41]. In this case, the intersections of the energy curves correspond to the regions of null energy [40].

3.2 Band Gap Structure. In this section, we consider laminates with incompressible electroelastic phases describing by the following energy potential:

$$\psi^{(\xi)}\left(\mathbf{F}^{(\xi)}, \mathbf{D}_L^{(\xi)}\right) = \psi_{\text{elas}}^{(\xi)}\left(I_1^{(\xi)}\right) + \frac{1}{2\varepsilon^{(\xi)}} I_5^{(\xi)} \tag{71}$$

where $I_1 = \text{tr}\mathbf{C} = \mathbf{F} : \mathbf{F}$ is the first invariant of the right Cauchy–Green deformation tensor $\mathbf{C} = \mathbf{F}^T \cdot \mathbf{F}$, and $I_5 = \mathbf{D}_L \cdot \mathbf{C} \cdot \mathbf{D}_L$ is the additional invariant accounting for the electromechanical coupling. The tensors of electroelastic moduli (15) for energy potential (71) are

$$\begin{aligned} \mathbb{C}_{ijkl}^{(\xi)} &= 2\left(\delta_{ik} B_{lj}^{(\xi)} \psi_1^{(\xi)} + 2B_{ij}^{(\xi)} B_{kl}^{(\xi)} \psi_{11}^{(\xi)}\right) + \frac{1}{\varepsilon^{(\xi)}} \delta_{ik} D_l^{(\xi)} D_j^{(\xi)}, \\ \boldsymbol{\mathcal{M}}_{ijk}^{(\xi)} &= \frac{1}{\varepsilon^{(\xi)}}\left(\delta_{ik} D_j^{(\xi)} + \delta_{jk} D_i^{(\xi)}\right), \quad K_{ij}^{(\xi)} = \frac{1}{\varepsilon^{(\xi)}} \delta_{ij} \end{aligned} \tag{72}$$

where $\psi_1^{(\xi)} = \partial\psi^{(\xi)}/\partial I_1^{(\xi)}$ and $\psi_{11}^{(\xi)} = \partial\psi_1^{(\xi)}/\partial I_1^{(\xi)}$.

We consider steady-state transversal small amplitude excitations propagating perpendicular to the interface between the layers (along the x_2 direction, see Fig. 1(*c*)) in the laminate subjected to macroscopically applied electromechanical loads

$$\bar{\mathbf{F}} = \lambda_1 \mathbf{e}_1 \otimes \mathbf{e}_1 + \lambda_2 \mathbf{e}_2 \otimes \mathbf{e}_2 + \lambda_3 \mathbf{e}_3 \otimes \mathbf{e}_3 \quad \text{and} \quad \bar{\mathbf{D}}_L = D_L \sqrt{\bar{\mu}\bar{\varepsilon}}\, \mathbf{e}_2 \tag{73}$$

Here, we use the displacement continuity along the interface between the layers (26) producing $\lambda_1^{(a)} = \lambda_1^{(b)} \equiv \lambda_1$ and $\lambda_3^{(a)} = \lambda_3^{(b)} \equiv \lambda_3$, and the incompressibility assumption yielding $\lambda_2^{(a)} = \lambda_2^{(b)} \equiv \lambda_2$. Following Tiersten [42], we assume that the incremental fields $\mathbf{u}^{(\xi)}$, $\dot{\mathbf{D}}_{L\star}^{(\xi)}$, and $\dot{p}^{(\xi)}$ depend on the coordinate x_2 and time t only. Under these assumptions, substitution of Eqs. (17), (18), and (72) into Eq. (12) yields

$$\frac{\partial^2 u_1^{(\xi)}}{\partial t^2} = \left(c_{\text{sw}}^{(\xi)}\right)^2 \frac{\partial^2 u_1^{(\xi)}}{\partial x_2^2}, \quad \frac{\partial \dot{p}^{(\xi)}}{\partial x_2} = 0, \text{ and } \frac{\partial^2 u_3^{(\xi)}}{\partial t^2} = \left(c_{\text{sw}}^{(\xi)}\right)^2 \frac{\partial^2 u_3^{(\xi)}}{\partial x_2^2} \tag{74}$$

where

$$c_{\text{sw}}^{(\xi)} = \lambda_2 \sqrt{2\psi_1^{(\xi)} \Big/ \rho^{(\xi)}} \tag{75}$$

Next, substitution of Eqs. (18), (72), and (73) into Eq. (17) yields

$$
\begin{aligned}
\dot{P}^{(\xi)}_{\star 12} &= 2\lambda_2^2\psi_1^{(\xi)}\frac{\partial u_1^{(\xi)}}{\partial x_2}+\frac{D_2^{(\xi)}}{\varepsilon^{(\xi)}}\left(D_2^{(\xi)}\frac{\partial u_1^{(\xi)}}{\partial x_2}+\dot{D}^{(\xi)}_{L\star 1}\right),\\
\dot{E}^{(\xi)}_{L\star 1} &= \frac{1}{\varepsilon^{(\xi)}}\left(D_2^{(\xi)}\frac{\partial u_1^{(\xi)}}{\partial x_2}+\dot{D}^{(\xi)}_{L\star 1}\right)\\
\dot{P}^{(\xi)}_{\star 22} &= \frac{2}{\varepsilon^{(\xi)}}D_2^{(\xi)}\dot{D}^{(\xi)}_{L\star 2}-\dot{p}^{(\xi)}\\
\dot{P}^{(\xi)}_{\star 32} &= 2\lambda_2^2\psi_1^{(\xi)}\frac{\partial u_3^{(\xi)}}{\partial x_2}+\frac{D_2^{(\xi)}}{\varepsilon^{(\xi)}}\left(D_2^{(\xi)}\frac{\partial u_3^{(\xi)}}{\partial x_2}+\dot{D}^{(\xi)}_{L\star 3}\right),\\
\dot{E}^{(\xi)}_{L\star 3} &= \frac{1}{\varepsilon^{(\xi)}}\left(D_2^{(\xi)}\frac{\partial u_3^{(\xi)}}{\partial x_2}+\dot{D}^{(\xi)}_{L\star 3}\right)
\end{aligned}
\tag{76}
$$

where $D_2^{(\xi)}=D_2$ according to Eq. $(29)_2$.

The incremental jump conditions across the interface between the layers ($x_2=0$) are

$$
\begin{aligned}
&\dot{P}^{(a)}_{\star 12}=\dot{P}^{(b)}_{\star 12},\quad \dot{P}^{(a)}_{\star 22}=\dot{P}^{(b)}_{\star 22},\quad \dot{P}^{(a)}_{\star 32}=\dot{P}^{(b)}_{\star 32},\\
&\dot{E}^{(a)}_{L\star 1}=\dot{E}^{(b)}_{L\star 1},\quad \dot{E}^{(a)}_{L\star 3}=\dot{E}^{(b)}_{L\star 3},\quad \dot{D}^{(a)}_{L\star 2}=\dot{D}^{(b)}_{L\star 2}
\end{aligned}
\tag{77}
$$

Hence, substitution of Eq. (76) into Eq. (77) yields

$$
\begin{aligned}
\psi_1^{(a)}\frac{\partial u_1^{(a)}}{\partial x_2}\bigg|_{x_2=0} &= \psi_1^{(b)}\frac{\partial u_1^{(b)}}{\partial x_2}\bigg|_{x_2=0},\\
\psi_1^{(a)}\frac{\partial u_3^{(a)}}{\partial x_2}\bigg|_{x_2=0} &= \psi_1^{(b)}\frac{\partial u_3^{(b)}}{\partial x_2}\bigg|_{x_2=0},\\
\dot{p}^{(b)}-\dot{p}^{(a)} &= D_2\dot{D}_{L\star 2}\left(\frac{1}{\varepsilon^{(b)}}-\frac{1}{\varepsilon^{(a)}}\right)
\end{aligned}
\tag{78}
$$

We seek solution for Eq. $(74)_1$ in the form

$$
u_1^{(\xi)}=A^{(\xi)}e^{i(k^{(\xi)}x_2-\omega t)}+B^{(\xi)}e^{i(-k^{(\xi)}x_2-\omega t)} \tag{79}
$$

where ω represents the angular frequency, and $k^{(\xi)}=\omega/c^{(\xi)}$ is the wave number. The perfect bonding between the layers implies

$$
u_1^{(a)}|_{x_2=0}=u_1^{(b)}|_{x_2=0} \tag{80}
$$

Then, the substitution of Eq. (79) into Eq. (80) yields

$$
A^{(a)}+B^{(a)}-A^{(b)}-B^{(b)}=0 \tag{81}
$$

Next, the substitution of Eq. (79) into Eq. $(78)_1$ yields

$$
\frac{\psi_1^{(a)}}{c^{(a)}}A^{(a)}-\frac{\psi_1^{(a)}}{c^{(a)}}B^{(a)}-\frac{\psi_1^{(b)}}{c^{(b)}}A^{(b)}+\frac{\psi_1^{(b)}}{c^{(b)}}B^{(b)}=0 \tag{82}
$$

Two additional conditions for constants $A^{(a)}$, $B^{(a)}$, $A^{(b)}$, and $B^{(b)}$ are obtained from the periodicity consideration. Hence, we adjust the form of the solution (79) to be the steady-state wave expression with the same wave number k for both phases

$$
u_1^{(\xi)}=U_1^{(\xi)}(x_2)e^{i(kx_2-\omega t)} \tag{83}
$$

where

$$
U_1^{(\xi)}(x_2)=A^{(\xi)}e^{iK_-^{(\xi)}x_2}+B^{(\xi)}e^{-iK_+^{(\xi)}x_2}\quad\text{and}\quad K_\pm^{(\xi)}=k^{(\xi)}\pm k \tag{84}
$$

According to Floquet theorem, functions $U_1^{(\xi)}(x_2)$ must be periodic with the period equal to the length of the unit cell (see Fig. 1(*c*)), namely $h=h^{(a)}+h^{(b)}$

$$
U_1^{(a)}(-h^{(a)})=U_1^{(b)}(h^{(b)}) \tag{85}
$$

Thus, substitution of Eq. (84) into Eq. (85) yields

$$
e^{-iK_-^{(a)}h^{(a)}}A^{(a)}+e^{iK_+^{(a)}h^{(a)}}B^{(a)}-e^{iK_-^{(b)}h^{(b)}}A^{(b)}-e^{-iK_+^{(b)}h^{(b)}}B^{(b)}=0 \tag{86}
$$

Next, substituting Eq. (83) and $\dot{D}^{(\xi)}_{L\star 1}=d_1^{(\xi)}(x_2)e^{i(kx_2-\omega t)}$ into Eq. $(76)_1$, we obtain

$$
\begin{aligned}
&\dot{E}^{(\xi)}_{L\star 1}(x_2,t)=\mathcal{E}_1^{(\xi)}(x_2)e^{i(kx_2-\omega t)},\\
&\mathcal{E}_1^{(\xi)}(x_2)=\frac{1}{\varepsilon^{(\xi)}}\left(D_2\frac{i\omega}{c^{(\xi)}}\left(A^{(\xi)}e^{iK_-^{(\xi)}x_2}-B^{(\xi)}e^{-iK_+^{(\xi)}x_2}\right)+d_1^{(\xi)}(x_2)\right)
\end{aligned}
\tag{87}
$$

and

$$
\begin{aligned}
&\dot{P}^{(\xi)}_{\star 12}(x_2,t)=\mathcal{P}_1^{(\xi)}(x_2)e^{i(kx_2-\omega t)},\\
&\mathcal{P}_1^{(\xi)}(x_2)=2\lambda_2^2\psi_1^{(\xi)}\frac{i\omega}{c^{(\xi)}}\left(A^{(\xi)}e^{iK_-^{(\xi)}x_2}-B^{(\xi)}e^{-iK_+^{(\xi)}x_2}\right)+D_2\mathcal{E}_1^{(\xi)}(x_2)
\end{aligned}
\tag{88}
$$

where according to Floquet theorem

$$
\begin{aligned}
&\mathcal{P}_1^{(a)}(-h^{(a)})=\mathcal{P}_1^{(b)}(h^{(b)}),\quad \mathcal{E}_1^{(a)}(-h^{(a)})=\mathcal{E}_1^{(b)}(h^{(b)}),\\
&d_1^{(a)}(-h^{(a)})=d_1^{(b)}(h^{(b)})
\end{aligned}
\tag{89}
$$

Finally, substitution of Eq. (88) into Eq. (89) yields

$$
\begin{aligned}
&\frac{\psi_1^{(a)}}{c^{(a)}}e^{-iK_-^{(a)}h^{(a)}}A^{(a)}-\frac{\psi_1^{(a)}}{c^{(a)}}e^{iK_+^{(a)}h^{(a)}}B^{(a)}-\frac{\psi_1^{(b)}}{c^{(b)}}e^{iK_-^{(b)}h^{(b)}}A^{(b)}\\
&\quad+\frac{\psi_1^{(b)}}{c^{(b)}}e^{-iK_+^{(b)}h^{(b)}}B^{(b)}=0
\end{aligned}
\tag{90}
$$

System of equations (81), (82), (86), and (90) has a nontrivial solution if

$$
\det\begin{bmatrix}
1 & 1 & -1 & -1\\
\dfrac{\psi_1^{(a)}}{c^{(a)}} & -\dfrac{\psi_1^{(a)}}{c^{(a)}} & -\dfrac{\psi_1^{(b)}}{c^{(b)}} & \dfrac{\psi_1^{(b)}}{c^{(b)}}\\
e^{-iK_-^{(a)}h^{(a)}} & e^{iK_+^{(a)}h^{(a)}} & -e^{iK_-^{(b)}h^{(b)}} & -e^{-iK_+^{(b)}h^{(b)}}\\
\dfrac{\psi_1^{(a)}}{c^{(a)}}e^{-iK_-^{(a)}h^{(a)}} & -\dfrac{\psi_1^{(a)}}{c^{(a)}}e^{iK_+^{(a)}h^{(a)}} & -\dfrac{\psi_1^{(b)}}{c^{(b)}}e^{iK_-^{(b)}h^{(b)}} & \dfrac{\psi_1^{(b)}}{c^{(b)}}e^{-iK_+^{(b)}h^{(b)}}
\end{bmatrix}=0
\tag{91}
$$

One can show that Eq. (91) together with Eq. (75) reduces to

$$
\begin{aligned}
\cos kh &= \cos\left(\frac{\omega h^{(a)}}{c^{(a)}}\right)\cos\left(\frac{\omega h^{(b)}}{c^{(b)}}\right)\\
&\quad-\frac{1}{2}\left(\frac{\rho^{(a)}c^{(a)}}{\rho^{(b)}c^{(b)}}+\frac{\rho^{(b)}c^{(b)}}{\rho^{(a)}c^{(a)}}\right)\sin\left(\frac{\omega h^{(a)}}{c^{(a)}}\right)\sin\left(\frac{\omega h^{(b)}}{c^{(b)}}\right)
\end{aligned}
\tag{92}
$$

describing the dispersion relation $\omega=\omega(k)$ with $c^{(\xi)}$ and $h^{(\xi)}$ being functions of deformation, which can be induced by electric field or otherwise, for example, purely mechanically. The obtained dispersion relation fully agrees with the exact solution for long waves (40) propagating perpendicular to the layers in electroelastic laminates, clearly showing that shear wave propagation is independent of electric field for this configuration. We note that the dispersion relation (92) is different from those presented

by Shmuel and deBotton [30,35] as detailed in the Appendix. Moreover, the dispersion relation (92) has the same form as the classical result for purely elastic laminates [34], if no deformation is applied. Recently, the dispersion relation by Rytov [34] has been extended to account for finite deformations in purely mechanical hyperelastic laminates [36]. Remarkably, the dispersion relation (92) is identical to the one considered in Galich et al. [36] for the purely mechanical problem; the only difference, which, however, does not affect the way how SBGs change, is that here the deformation is induced by an electric field. Thus, the analysis and conclusions of Galich et al. [36] can be fully applied here. In particular, Galich et al. [36] showed that SBGs do not depend on deformation in laminates with neo-Hookean phases. This is due to the fact that the two main factors—changes in the geometry and phase velocity induced by deformation—completely cancel each other [36]. This is again in contradiction with the conclusions of Shmuel and deBotton [30,35], and Shmuel and Band [43]; these works utilized different dispersion relations, but all arrived at the conclusions that SBGs are tunable by an electric field [30,35] or by deformation [43] in neo-Hookean ideal dielectric or purely mechanical neo-Hookean laminates, respectively. Once again, the SBGs do not depend either on deformation or on electric field in the neo-Hookean ideal dielectric or purely mechanical neo-Hookean laminates.

To achieve electric field (or deformation)-induced tunability of the SBGs, one should consider laminates with phases exhibiting stronger stiffening, for example, Arruda–Boyce [44] or Gent [45] phases. To illustrate this, we consider laminates with electroelastic phases describing by the energy potential (71) with Gent elastic part [45]

$$\psi_{\text{elas}}^{(\xi)}(\mathbf{F}^{(\xi)}) = -\frac{\mu^{(\xi)} J_m^{(\xi)}}{2} \ln\left(1 - \frac{I_1^{(\xi)} - 3}{J_m^{(\xi)}}\right) \tag{93}$$

where $J_m^{(\xi)}$ is the dimensionless parameter defining the lock-up stretch ratio, such that in the limit $(I_1^{(\xi)} - 3) \to J_m^{(\xi)}$, the strain energy becomes unbounded. Recall that the stiffening effects describing by the Gent model, which is an approximation of the Arruda–Boyce model [44], refer to finite extensibility of polymer chains. For DE laminates with electroelastic Gent phases subjected to the electric field perpendicular to the layers (as defined in Eq. (47)), the relation between the induced stretch and Lagrangian electric displacement is

$$D_L = \lambda^{-1} \sqrt{\frac{\lambda^3 - 1}{\bar{\mu}} \left(\frac{J_m^{(a)} \nu^{(a)} \mu^{(a)}}{2 - \left(3 + J_m^{(a)}\right)\lambda + \lambda^3} + \frac{J_m^{(b)} \nu^{(b)} \mu^{(b)}}{2 - \left(3 + J_m^{(b)}\right)\lambda + \lambda^3} \right)} \tag{94}$$

Substitution of Eq. (93) into Eq. (75) yields [8]

$$c_G^{(\xi)} = \lambda \sqrt{\frac{J_m^{(\xi)}}{3 + J_m^{(\xi)} - \lambda^2 - 2\lambda^{-1}} \frac{\mu^{(\xi)}}{\rho^{(\xi)}}} \tag{95}$$

Next, by making use of Eqs. (94), (95), (24), and (92), SBG structures can be constructed for electroelastic laminates subjected to the electric field perpendicular to the layers. Figures 6(*a*)–6(*c*) show the SBGs as functions of the Lagrangian electric displacement applied perpendicular to the layers for wave propagating perpendicular to the layers in the DE laminates with the Gent electroelastic phases. Thanks to the specific normalization of the Lagrangian electric displacement, namely $\bar{\mathbf{D}}_L = D_L \sqrt{\bar{\mu}\bar{\varepsilon}}\, \mathbf{e}_2$, the presented band gaps correspond to DE laminates with any contrast in electric permittivities $\varepsilon^{(a)}/\varepsilon^{(b)}$ between the layers. The lock-up stretch for $J_m = 0.5$ is $\lambda_{\text{lock}} \simeq 0.65$. Application of $D_L = 3.5$ leads the contraction of the considered DE laminates down to $\lambda \simeq 0.68$. Clearly, the application of the electric field perpendicular to the layers widens and shifts SBGs up to the higher frequencies. In particular, the application of the Lagrangian electric displacement of $D_L = 3.5$ to the laminate with $\nu^{(a)} = 0.5$ and $\mu^{(a)}/\mu^{(b)} = 10$ shifts the lower boundary of the first SBG from $f_n = 0.41$ up to

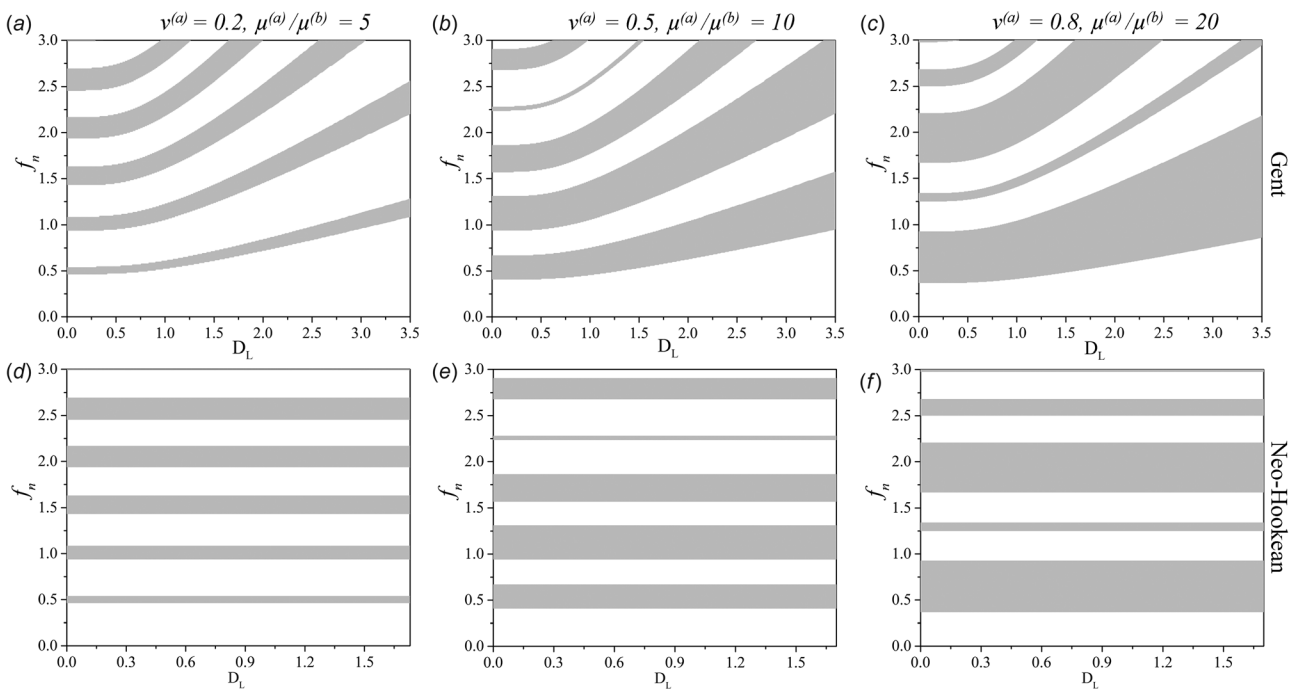

Fig. 6 Shear wave band gaps as functions of dimensionless Lagrangian electric displacement for waves propagating perpendicular to the layers. The band gap structures are true for any contrast in electric permittivities $\varepsilon^{(a)}/\varepsilon^{(b)}$ between the layers. The locking parameters for Gent phases are $J_m^{(a)} = J_m^{(b)} = 0.5$. The densities of the layers are identical, i.e., $\rho^{(a)}/\rho^{(b)} = 1$. Frequency is normalized as $f_n = (\omega H/2\pi)\sqrt{\bar{\rho}/\bar{\mu}}$.

$f_n = 0.95$ and widens it from $\Delta f_n = 0.26$ up to $\Delta f_n = 0.62$ (see Fig. 6(*b*)). Once again, these changes in SBGs occur due to electrostatically induced deformation. As a comparison, Figs. 6(*d*)–6(*f*) show the SBGs as functions of the Lagrangian electric displacement applied perpendicular to the layers for the waves propagating perpendicular to the layers in the DE laminates with the neo-Hookean electroelastic phases. Recall that for the neo-Hookean dielectric elastomer laminates, the normalized limiting electric displacement is constant, i.e., $D_L^{\lim} = \sqrt{3}$, while for the Gent dielectric elastomer laminates, the limiting electric field depends on the on the locking parameter J_m. Note that for the Gent DE laminates discussed in Fig. 6, the limiting electric fields are higher than the ones needed to reach the lock-up stretches. Finally, we note that the influence of stiffening effects on band gap structures in finitely deformed incompressible and compressible layered materials was thoroughly analyzed by Galich et al. [36]. The only difference is that here we induce deformation by application of an electric field.

4 Conclusion

We considered shear wave propagation in electroelastic layered media subjected to finite deformations and electric fields. First, we derived the long wave estimates—the exact solution for the long waves—for phase and group velocities of shear waves propagating in the laminates with electroelastic neo-Hookean phases. The derived formulae are expressed in terms of the volume fractions and electroelastic constants of the phases. Moreover, these long wave estimates are given for any direction of wave propagation, and for any applied electric field and homogenous finite deformations. Furthermore, we have found that the shear wave propagation perpendicular to the layers depends on electric field only though the induced deformation.

Second, we derived the dispersion relations for the shear waves propagating perpendicular to the layers in the laminates with incompressible hyperelastic ideal dielectric phases, described by the energy potential (71). Consistently with the long wave estimates, the derived dispersion relation is independent of electric field, and the dispersion relation has the same form as its analog for the purely elastic laminates. The dispersion relation shows that SBGs in the electroelastic laminates are tunable by an electric field only through induced deformation. In particular, the application of an electric field to the DE laminates with electroelastic Gent phases widens and shifts SBGs toward higher frequencies. However, SBGs do not depend on deformation (induced by an electric field or mechanically) in DE laminates with electroelastic neo-Hookean phases. Finally, we emphasize that consideration of dissipation can potentially improve the accuracy of the predictions, especially for the composites with constituents characterized by strong damping effects [46].

Acknowledgment

S.R. thanks the support of Taub Foundation through the Horev Fellowship—Leaders in Science and Technology. P.G. thanks the support through the Jacobs Fellowship.

Funding Data

- Israel Science Foundation (1550/15).

Appendix: Comparison of Dispersion Relation, Exact Solution for Long Waves, and Results by Shmuel and deBotton

Figure 7 shows a comparison of the exact solution for long waves (59), dispersion relation (92), and the results reported by Shmuel and deBotton [30,35]. For clarity, we normalize the wave vector and frequency as in Shmuel and deBotton [30]. The DE laminate is subjected to the electrostatic excitation of $D_L = 1.27$ (corresponding to $\hat{D} = 1.5$ in Shmuel and deBotton [30,35]). The continuous black and dotted blue curves correspond to the exact solution for long waves (59) and dispersion relation (92), respectively. The dotted and dashed red curves refer to the results reported by Shmuel and deBotton [30] (see Fig. 8(*a*) therein) and the results presented in Shmuel and deBotton [35] (see Fig. 7(*b*) therein), respectively. We observe that the curves for dispersion relation (92) and exact solution for long waves (59) overlap, while the dispersion curves from Shmuel and deBotton [30,35] significantly differ from the exact solution for long waves.

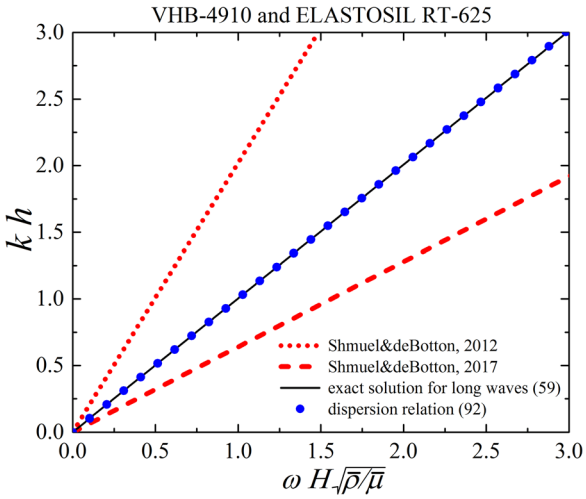

Fig. 7 Comparison of the exact solution for long waves (59), dispersion relation (92), and results reported by Shmuel and deBotton [30,35] for the shear waves propagating perpendicular to the layers in the laminates with incompressible ideal DE neo-Hookean phases subjected to electric field perpendicular to layers, namely $D_L = 1.27$. The laminate is made of VHB-4910 and ELASTOSIL RT-625: $\nu^{(a)} = 0.5$, $\mu^{(a)}/\mu^{(b)} = 1.19$, $\varepsilon^{(a)}/\varepsilon^{(b)} = 1.74$, and $\rho^{(a)}/\rho^{(b)} = 0.94$, where $\mu^{(b)} = 342$ kPa, $\varepsilon^{(b)} = 2.7$, and $\rho^{(b)} = 1020$ kg/m^3.

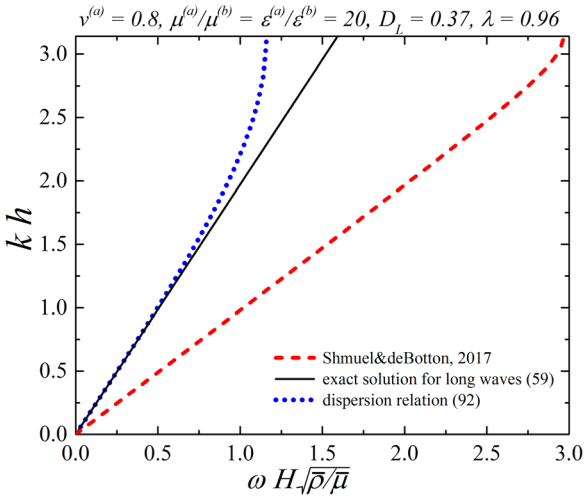

Fig. 8 Comparison of the exact solution for long waves (59), dispersion relation (92), and dispersion relation by Shmuel and deBotton [35] for the waves propagating perpendicular to the layers in the laminates with incompressible neo-Hookean phases subjected to electric field perpendicular to layers, namely, $D_L = 0.37$, $\nu^{(a)} = 0.8$, $\mu^{(a)}/\mu^{(b)} = \varepsilon^{(a)}/\varepsilon^{(b)} = 20$, and $\rho^{(a)}/\rho^{(b)} = 1$

For completeness, we show a comparison of the exact solution for long waves (59), dispersion relation (92), and dispersion relation reported by Shmuel and deBotton [35] for the DE laminates with a more pronounced dispersion. In particular, the comparison is shown for the DE laminates with incompressible neo-Hookean phases with $\nu^{(a)} = 0.8$, $\mu^{(a)}/\mu^{(b)} = \varepsilon^{(a)}/\varepsilon^{(b)} = 20$, and $\rho^{(a)}/\rho^{(b)} = 1$ in Fig. 8. The laminate is subjected to the electric field perpendicular to the layers, namely, $D_L = 0.37$ (corresponding to $\hat{D} = 3$ in the notation of Shmuel and deBotton [35]). We observe that dispersion relation (92) and the exact solution for long waves (59) are in excellent agreement for the corresponding wavelengths, whereas the results reported by Shmuel and deBotton [35] produce significantly different results from the exact solution for long waves (59) even in the long wave limit of $kh \to 0$. In particular, for this case, the phase velocity predicted by the exact solution (59) significantly differs from the phase velocity calculated from the dispersion relation by Shmuel and deBotton [35] by a factor of 2, namely, $\bar{c}^{(\mathrm{SD})} \simeq 2\bar{c}_{\mathrm{sw}}$.

References

[1] Pelrine, R., Kornbluh, R., Pei, Q.-B., and Joseph, J., 2000, "High-Speed Electrically Actuated Elastomers With Strain Greater Than 100%," Science, **287**(5454), pp. 836–839.

[2] Bar-Cohen, Y., 2004, *Electroactive Polymer (EAP) Actuators as Artificial Muscles: Reality, Potential, and Challenges*, Vol. 136, SPIE Press, Bellingham, WA.

[3] Rudykh, S., Bhattacharya, K., and deBotton, G., 2012, "Snap-Through Actuation of Thick-Wall Electroactive Balloons," Int. J. Nonlinear Mech., **47**(2), pp. 206–209.

[4] Li, T., Keplinger, C., Baumgartner, R., Bauer, S., Yang, W., and Suo, Z., 2013, "Giant Voltage-Induced Deformation in Dielectric Elastomers Near the Verge of Snap-Through Instability," J. Mech. Phys. Solids, **61**(2), pp. 611–628.

[5] McKay, T., O'Brien, B., Calius, E., and Anderson, I., 2010, "An Integrated, Self-Priming Dielectric Elastomer Generator," Appl. Phys. Lett., **97**(6), p. 062911.

[6] Kornbluh, R. D., Pelrine, R., Prahlad, H., Wong-Foy, A., McCoy, B., Kim, S., Eckerle, J., and Low, T., 2012, "From Boots to Buoys: Promises and Challenges of Dielectric Elastomer Energy Harvesting," *Electroactivity in Polymeric Materials*, Springer, Berlin, pp. 67–93.

[7] Rudykh, S., and Boyce, M., 2014, "Transforming Wave Propagation in Layered Media Via Instability-Induced Interfacial Wrinkling," Phys. Rev. Lett., **112**(3), p. 034301.

[8] Galich, P. I., and Rudykh, S., 2015, "Influence of Stiffening on Elastic Wave Propagation in Extremely Deformed Soft Matter: From Nearly Incompressible to Auxetic Materials," Extreme Mech. Lett., **4**, pp. 156–161.

[9] Galich, P. I., and Rudykh, S., 2015, "Comment on "Disentangling Longitudinal and Shear Elastic Waves by neo-Hookean Soft Devices" [Appl. Phys. Lett., 106, 161903 (2015)]," Appl. Phys. Lett., **107**(5), p. 056101.

[10] Galich, P. I., Slesarenko, V., and Rudykh, S., 2017, "Shear Wave Propagation in Finitely Deformed 3D Fiber-Reinforced Composites," Int. J. Solids Struct., **110–111**, pp. 294–304.

[11] Gei, M., Roccabianca, S., and Bacca, M., 2011, "Controlling Bandgap in Electroactive Polymer-Based Structures," IEEE/ASME Trans. Mechatronics, **16**(1), pp. 102–107.

[12] Galich, P. I., and Rudykh, S., 2016, "Manipulating Pressure and Shear Elastic Waves in Dielectric Elastomers Via External Electric Stimuli," Int. J. Solids Struct., **91**, pp. 18–25.

[13] Wu, B., Su, Y., Chen, W., and Zhang, C., 2017, "On Guided Circumferential Waves in Soft Electroactive Tubes Under Radially Inhomogeneous Biasing Fields," J. Mech. Phys. Solids, **99**, pp. 116–145.

[14] Yang, W.-P., and Chen, L.-W., 2008, "The Tunable Acoustic Band Gaps of Two-Dimensional Phononic Crystals With a Dielectric Elastomer Cylindrical Actuator," Smart Mater. Struct., **17**(1), p. 015011.

[15] Celli, P., Gonella, S., Tajeddini, V., Muliana, A., Ahmed, S., and Ounaies, Z., 2017, "Wave Control Through Soft Microstructural Curling: Bandgap Shifting, Reconfigurable Anisotropy and Switchable Chirality," Smart Mater. Struct., **26**(3), p. 035001.

[16] Toupin, R. A., 1956, "The Elastic Dielectric," Arch. Ration. Mech. Anal., **5**, pp. 849–915.

[17] Dorfmann, A., and Ogden, R. W., 2005, "Nonlinear Electroelasticity," Acta. Mech., **174**(3–4), pp. 167–183.

[18] McMeeking, R. M., and Landis, C. M., 2005, "Electrostatic Forces and Stored Energy for Deformable Dielectric Materials," ASME J. Appl. Mech., **72**(4), pp. 581–590.

[19] Suo, Z., Zhao, X., and Greene, W. H., 2008, "A Nonlinear Field Theory of Deformable Dielectrics," J. Mech. Phys. Solids, **56**(2), pp. 467–486.

[20] Cohen, N., Dayal, K., and deBotton, G., 2016, "Electroelasticity of Polymer Networks," J. Mech. Phys. Solids, **92**, pp. 105–126.

[21] deBotton, G., Tevet-Deree, L., and Socolsky, E. A., 2007, "Electroactive Heterogeneous Polymers: Analysis and Applications to Laminated Composites," Mech. Adv. Mater. Struct., **14**(1), pp. 13–22.

[22] Tian, L., Tevet-Deree, L., deBotton, G., and Bhattacharya, K., 2012, "Dielectric Elastomer Composites," J. Mech. Phys. Solids, **60**(1), pp. 181–198.

[23] Rudykh, S., Lewinstein, A., Uner, G., and deBotton, G., 2013, "Analysis of Microstructural Induced Enhancement of Electromechanical Coupling in Soft Dielectrics," Appl. Phys. Lett., **102**(15), p. 151905.

[24] Rudykh, S., and deBotton, G., 2011, "Stability of Anisotropic Electroactive Polymers With Application to Layered Media," Z. Angew. Math. Phys., **62**(6), pp. 1131–1142.

[25] Bertoldi, K., and Gei, M., 2011, "Instabilities in Multilayered Soft Dielectrics," J. Mech. Phys. Solids, **59**(1), pp. 18–42.

[26] Rudykh, S., Bhattacharya, K., and deBotton, G., 2014, "Multiscale Instabilities in Soft Heterogeneous Dielectric Elastomers," Proc. R. Soc. A, **470**(2162), p. 20130618.

[27] Abu-Salih, S., 2017, "Analytical Study of Electromechanical Buckling of a Micro Spherical Elastic Film on a Compliant Substrate—Part I: Formulation and Linear Buckling of Periodic Patterns," Int. J. Solids Struct., **109**, pp. 180–188.

[28] Goshkoderia, A., and Rudykh, S., 2017, "Electromechanical Macroscopic Instabilities in Soft Dielectric Elastomer Composites With Periodic Microstructures," Eur. J. Mech. A, **65**, pp. 243–256.

[29] Dorfmann, A., and Ogden, R. W., 2010, "Electroelastic Waves in a Finitely Deformed Electroactive Material," IMA J. Appl. Math., **75**(4), pp. 603–636.

[30] Shmuel, G., and deBotton, G., 2012, "Band-Gaps in Electrostatically Controlled Dielectric Laminates Subjected to Incremental Shear Motions," J. Mech. Phys. Solids, **60**(11), pp. 1970–1981.

[31] Kolle, M., Lethbridge, A., Kreysing, M., Baumberg, J., Aizenberg, J., and Vukusic, P., 2013, "Bio-Inspired Band-Gap Tunable Elastic Optical Multilayer Fibers," Adv. Mater., **25**(15), pp. 2239–2245.

[32] Rudykh, S., Ortiz, C., and Boyce, M., 2015, "Flexibility and Protection by Design: Imbricated Hybrid Microstructures of Bio-Inspired Armor," Soft Matter, **11**(13), pp. 2547–2554.

[33] Slesarenko, V., and Rudykh, S., 2016, "Harnessing Viscoelasticity and Instabilities for Tuning Wavy Patterns in Soft Layered Composites," Soft Matter, **12**(16), pp. 3677–3682.

[34] Rytov, S., 1956, "Acoustical Properties of a Thinly Laminated Medium," Sov. Phys. Acoust., **2**, pp. 68–80.

[35] Shmuel, G., and deBotton, G., 2017, "Corrigendum to 'Band-Gaps in Electrostatically Controlled Dielectric Laminates Subjected to Incremental Shear Motions' [J. Mech. Phys. Solids, 60 (2012) 1970–1981]," J. Mech. Phys. Solids, **105**, pp. 21–24.

[36] Galich, P. I., Fang, N. X., Boyce, M. C., and Rudykh, S., 2017, "Elastic Wave Propagation in Finitely Deformed Layered Materials," J. Mech. Phys. Solids, **98**, pp. 390–410.

[37] Spinelli, S. A., and Lopez-Pamies, O., 2015, "Some Simple Explicit Results for the Elastic Dielectric Properties and Stability of Layered Composites," Int. J. Eng. Sci., **88**, pp. 15–28.

[38] Zhao, X., Hong, W., and Suo, Z., 2007, "Electromechanical Hysteresis and Coexistent States in Dielectric Elastomers," Phys. Rev. B, **76**(13), p. 134113.

[39] Musgrave, M., 1970, *Crystal Acoustics: Introduction to the Study of Elastic Waves and Vibrations in Crystals*, Holden-Day, San Francisco, CA.

[40] Nayfeh, A. H., 1995, *Wave Propagation in Layered Anisotropic Media: With Applications to Composites*, Elsevier Science, New York.

[41] Langenberg, K. J., Marklein, R., and Mayer, K., 2010, "Energy vs. Group Velocity for Elastic Waves in Homogeneous Anisotropic Solid Media," IEEE URSI International Symposium on Electromagnetic Theory (EMTS), Berlin, Aug. 16–19, pp. 733–736.

[42] Tiersten, H. F., 1963, "Thickness Vibrations of Piezoelectric Plates," J. Acoust. Soc. Am., **35**(1), pp. 53–58.

[43] Shmuel, G., and Band, R., 2016, "Universality of the Frequency Spectrum of Laminates," J. Mech. Phys. Solids, **92**, pp. 127–136.

[44] Arruda, E. M., and Boyce, M. C., 1993, "A Three-Dimensional Constitutive Model for the Large Stretch Behavior of Rubber Elastic Materials," J. Mech. Phys. Solids, **41**(2), pp. 389–412.

[45] Gent, A. N., 1996, "A New Constitutive Relation for Rubber," Rubber Chem. Technol., **69**(1), pp. 59–61.

[46] Babaee, S., Wang, P., and Bertoldi, K., 2015, "Three-Dimensional Adaptive Soft Phononic Crystals," J. Appl. Phys., **117**(24), p. 244903.